6

Applications to steady problems

The focus will now shift away from discussion of estimation methods in a somewhat abstract context, to more specific applications, primarily for large-scale fluid flows, and to the ocean in particular. When the first edition of this book (OCIP[1]) was written, oceanographic uses of the methods described here were still extremely unfamiliar to many, and they retained an aura of controversy. Controversy arose for two reasons: determining the ocean circulation was a classical problem that had been discussed with ideas and methods that had hardly changed in 100 years; the introduction of algebraic and computer methods seemed to many to be an unwelcome alien graft onto an old and familiar problem. Second, some of the results of the use of these methods were so at odds with "what everyone knew," that those results were rejected out of hand as being obviously wrong – with the methods being assumed flawed.

In the intervening 25+ years, both the methodology and the inferences drawn have become more familiar and less threatening. This change in outlook permits the present chapter to focus much less on the why and how of such methods in the oceanographic context, and much more on specific examples of how they have been used.[2] Time-dependent problems and methods will be discussed in Chapter 7.

This chapter is not intended to be an oceanographic textbook, but does outline the so-called geostrophic inverse problem. The chapter should be accessible even to those without any oceanographic knowledge: the problems are primarily those of making inferences from tracers in a large-scale fluid flow. Anyone seeking understanding of the oceanographic details should consult one of the references provided in the text.

Inverse methods were introduced into oceanography by the need to determine the ocean circulation from large-scale hydrographic data. At that time (the middle 1970s), the focus was still on determining a "mean" circulation based on data obtained from ships over timescales ranging from weeks to decades. Ironically, much of the interest in this problem has waned in the intervening years, as it became

obvious that the ocean is highly time-dependent. The fiction that the flow could be regarded as steady over arbitrarily long periods became increasingly difficult to sustain in the teeth of increasing evidence to the contrary. It is still useful, nonetheless, to study this problem in some depth: (1) A very large literature is focussed on it, and the steady-state approximation is sometimes sufficiently accurate to provide useful information about the circulation. (2) Interpretation of the time-dependent problem, both in terms of the methodology, and of the physics, depends upon understanding the steady-flow results. As with most approximations in science, however, one must always bear in mind the limitations of the result.

We begin with a review of the steady tracer problem, one applicable to a wide class of fluid-flow problems, and then turn to the ocean circulation problem.

6.1 Steady-state tracer distributions

A generic distribution equation for tracer C in steady state is

$$\mathbf{v} \cdot \boldsymbol{\nabla} C - \boldsymbol{\nabla} (\mathbf{K} \boldsymbol{\nabla} C) = -\lambda C + m_C(\mathbf{r}). \tag{6.1}$$

Here the velocity field, $\mathbf{v}(\mathbf{r})$, can be one- to three-dimensional (in one dimension it is a "pipeflow"), and will in general be a function of the spatial coordinate $\mathbf{r}$. The mixing tensor, $\mathbf{K}$, can also be dependent upon position and is often anisotropic because it represents a parameterization of subgridscale (eddy) mixing processes sometimes greatly influenced by fluid stratification or geometry. ($\mathbf{K}$ could be the molecular value, which would thus be a special case with its value known nearly perfectly.) λC is present to permit the study of tracers (carbon-14 is an example) undergoing radioactive decay. Finally, $m_C(\mathbf{r})$ represents any interior sources and sinks of C other than radio-decay. In the most general situation, m_C can be a function of C, permitting representation of chemical reaction terms.

Equation (6.1) is bilinear in $([\mathbf{v}, \mathbf{K}], C)$ – that is, with $[\mathbf{v}, \mathbf{K}]$ known, it is linear in C, and if C is known, it is linear in $[\mathbf{v}, \mathbf{K}]$. It thus lends itself to two distinct classes of linear inverse problem, depending upon which of $[\mathbf{v}, \mathbf{K}]$, or C is regarded as known/unknown. Usually, however, one has imperfect knowledge of both sets and any resulting inverse problem will be non-linear to some degree (m_C, if partly unknown, does not usually render the problem non-linear).

The most common application of steady tracer distributions has been in so-called box models, where integral versions of Eq. (6.1) have been used, as in the example on p. 10, to describe *net* exchanges between large reservoirs, without distinguishing between tracer movement by way of advection, $\mathbf{v}$, and by diffusion, $\mathbf{K}$. Most such models have been used in forward mode alone (recall, from Chapter 1, that "forward" or "direct" mode refers to the conventional well-posed initial/boundary value problem).

Box models are powerful tools for obtaining scale analyses for order of magnitude estimates of exchange rates. They often suffer from an underparameterization of the possible flow paths, and, consequently, can lead to grossly incorrect inferences. Consider the minimal reservoir problem (p. 59), in which a volume V_0 with tracer concentration C_0 is supposed fed from two reservoirs of concentration C_1, C_2, such that $C_1 \leq C_0 \leq C_2$. It was found that assuming two feeding reservoirs produced a definitive answer. If, however, one was suspicious of the existence of a third (or more) feeding reservoir, it was found that formulating the problem so as to deal with the indeterminacy was a better strategy than simply pretending it was not possible.

Another common approach to inferences from steady tracers is exemplified by the calculation of Munk (1966), for a one-dimensional pipeflow, using a representation of two tracers in vertical balance given by

$$w\frac{\partial C_1}{\partial z} - k\frac{\partial^2 C_1}{\partial z^2} = 0, \tag{6.2}$$

$$w\frac{\partial C_2}{\partial z} - k\frac{\partial^2 C_2}{\partial z^2} = -\lambda C_2, \tag{6.3}$$

where C_1 is temperature and C_2 is radiocarbon, ^{14}C. Because a one-dimensional balance is assumed, the flow, w, must be a constant, and the problem was further simplified by assuming the turbulent mixing coefficient $k =$ constant. By fitting observations of $C_1(z)$, $C_2(z)$ at one location in the central Pacific Ocean, and representing $\partial C_i/\partial z$, $\partial^2 C_i/\partial z^2$ as fixed, known, constants with depth, Munk (1966) reduced Eqs. (6.2) and (6.3) to two equations in two unknowns, $[w, k]$, that is, as

$$\mathbf{Ex} + \mathbf{n} = \mathbf{y},$$

although no formal uncertainty estimate was provided. The missing error analysis of this solution was later provided by Olbers and Wenzel (1989) who found that the calculation was nearly singular.

Wunsch (1985) and McIntosh and Veronis (1993) discuss a finite difference form of Eq. (6.1) in two dimensions. On a grid with Δx, Δy, and using indices i, j, one has

$$\begin{aligned}(C_{i+1,j} + C_{i,j})u_{i,j} - (C_{i,j} + C_{i-1,j})u_{i-1,j} \\ + \delta[(C_{i,j+1} + C_{i,j})v_{i,j} - (C_{i,j} + C_{i,j-1})v_{i,j-1}] \\ = 2K/\Delta x[C_{i+1,j} + C_{i-1,j} - 2C_{i,j} + \delta^2(C_{i,j+1} + C_{i,j-1} - 2C_{i,j})],\end{aligned} \tag{6.4}$$

subject to the continuity relation

$$u_{i,j} - u_{i-1,j} + \delta(v_{i,j} - v_{i,j-1}) = 0, \qquad \delta = \Delta y/\Delta x. \tag{6.5}$$

Solution of this set of simultaneous equations for various assumptions concerning C_{ij} for u_{ij}, v_{ij} are discussed by Wunsch (1985) and McIntosh and Veronis (1993). The latter authors employ a streamfunction for the velocity, $u = \partial\psi/\partial y$, $v = -\partial\psi/\partial x$, and explore the use of weighting functions in least-squares that attempt (recall Eq. (2.134)) to find the smoothest possible solutions. As noted previously, with least-squares one can invoke any desired aesthetic principle for the solution, as long as it can be expressed through a weight matrix. It is for this reason that least-squares is best regarded as a curve-fitting procedure, rather than as an estimation one, unless the weight matrices are chosen specifically to produce the same solution as does the Gauss–Markov result.

6.2 The steady ocean circulation inverse problem

6.2.1 Equations of motion

The ocean circulation is governed by Newton's laws of motion plus those of the thermodynamics of a heat- and salt-stratified fluid. That these physics govern the system is a concise statement that a great deal is known about it. One seeks to exploit this information to the fullest extent possible, combining this theoretical knowledge with whatever observations are available.

The resulting equations of motion describing the ocean are the so-called Navier–Stokes equations for a thin shell of temperature- and salinity-stratified fluid on a bumpy, near-spheroidal body undergoing rapid rotation, augmented with an equation of state for density. Appropriate boundary conditions are those of no flow of fluid into the bottom and sides, statements about the stress exerted on these boundaries, and those representing exchange of momentum, heat, and moisture with the atmosphere at the surface. So-called tracer advection equations govern the distributions of temperature, salt, oxygen, and other scalar properties. The science of oceanography is in large part occupied with finding simplifications of this complicated system of equations adequate to provide description, understanding, and, ultimately, forecasting where possible.

6.2.2 Geostrophy

Local Cartesian approximations to the full equations are sufficient for many purposes. Both theory and decades of ocean observation lead to the inference that local

"geostrophic, hydrostatic" balance is an excellent approximation:

$$-\rho(x,y,z,t)\,f(y)\,v(x,y,z,t) = -\frac{\partial p(x,y,z,t)}{\partial x}, \tag{6.6}$$

$$\rho(x,y,z,t)\,f(y)\,u(x,y,z,t) = -\frac{\partial p(x,y,z,t)}{\partial y}, \tag{6.7}$$

$$0 = -\frac{\partial p(x,y,z,t)}{\partial z} - g\rho(x,y,z,t), \tag{6.8}$$

where p is the pressure (Eq. (6.8) asserts that it is hydrostatic); u, v are the zonal (x-direction), and meridional (y-direction) flow fields; $\rho(x,y,z)$ is the fluid density; g is local gravity; and $f = 2\Omega\sin\phi$ is the Coriolis parameter, where ϕ is the local latitude and Ω is the Earth's rotation rate (radians/second). One commonly writes $f = f_0 + \beta y$ to account for its local dependence on latitude. *The reader is cautioned that x, y are here spatial coordinates and should not be confused with* $\mathbf{x}$*, the state vector, or* $\mathbf{y}$*, the observation vector, used previously*. This convention for spatial coordinates is so deeply embedded in the literature that it seems quixotic to not use it here. (The time, t, has been placed into the arguments in the above equation as a reminder that these balances are often excellent ones, even in a time-evolving field.) The above equations are not exact, but they are so close to balancing that observational tests of their differences almost universally fail. On the other hand, the small deviations from precise equality are essential to determining oceanic physics.[3]

Defining w to be the local vertical velocity, approximate mass conservation is readily shown to be equivalent to

$$\frac{\partial u}{\partial x} + \frac{\partial v}{\partial y} + \frac{\partial w}{\partial z} = 0, \tag{6.9}$$

and conservation of density is

$$u\frac{\partial \rho}{\partial x} + v\frac{\partial \rho}{\partial y} + w\frac{\partial \rho}{\partial z} = 0, \tag{6.10}$$

(a special case of Eq. (6.1)) or, if combined with (6.9),

$$\frac{\partial(\rho u)}{\partial x} + \frac{\partial(\rho v)}{\partial y} + \frac{\partial(\rho w)}{\partial z} = 0. \tag{6.11}$$

The equation of state,

$$\rho(x,y,z,t) = \varrho(T(x,y,z,t), S(x,y,z,T), p(x,y,z,t)), \tag{6.12}$$

is an empirical relationship for density ρ in terms of local temperature, T, salinity, S, and pressure, p.

Without diffusion, tracer conservation can be written as

$$u\frac{\partial(\rho C)}{\partial x}+v\frac{\partial(\rho C)}{\partial y}+w\frac{\partial(\rho C)}{\partial z}=m_C(x,y,z,t), \tag{6.13}$$

or, if combined with (6.9), as

$$\frac{\partial(\rho Cu)}{\partial x}+\frac{\partial(\rho Cv)}{\partial y}+\frac{\partial(\rho Cw)}{\partial z}=m_C(x,y,z,t), \tag{6.14}$$

where m_C is a generic trace source or sink. For readers unfamiliar with, or uninterested in, the ocean, the equations (6.6)–(6.14) should simply be taken as axiomatic relations among physical variables.

The classical dynamic method

The "thermal wind equations" are obtained from (6.6)–(6.8) by cross-differentiation to eliminate the pressure,

$$-f\frac{\partial(\rho v)}{\partial z}=g\frac{\partial\rho}{\partial x}, \tag{6.15}$$

$$f\frac{\partial(\rho u)}{\partial z}=g\frac{\partial\rho}{\partial y}, \tag{6.16}$$

and can be integrated in the vertical to produce

$$\begin{aligned}\rho u(x,y,z,t)&=\frac{g}{f}\int_{z_0}^{z}\frac{\partial\rho}{\partial y}\mathrm{d}z+\rho c(x,y,t,z_0)\\&\equiv\rho\,(x,y,z,t)\,[u_R\,(x,y,z,t)+c(x,y,z_0,t)],\end{aligned} \tag{6.17}$$

$$\begin{aligned}\rho v(x,y,z,t)&=-\frac{g}{f}\int_{z_0}^{z}\frac{\partial\rho}{\partial x}\mathrm{d}z+\rho b(x,y,t,z_0)\\&\equiv\rho(x,y,z,t)[v_R(x,y,z,t)+b(x,y,z_0,t)].\end{aligned} \tag{6.18}$$

Depth, z_0, is the "reference depth" and is arbitrary. Note that the two integration constants b, c do not depend upon z, but only upon the fixed value z_0. u_R, v_R are the "relative velocities," and the integration constants b, c are the "reference-level velocities."

From the middle of the nineteenth century, scientists learned to measure T, S as functions of depth (usually determined from the pressure via the hydrostatic equation) at sea permitting the computation of $\rho\,(x,y,z,t)$. From Eqs. (6.17) and (6.18) calculation of the velocity follows – except for the contribution from b, c. Apart from that portion, the geostrophic flow can then be calculated from shipboard measurements of the horizontal derivatives of ρ alone. The integration constants – that is, the reference level velocities – are mathematically simple, but the inability to determine them plagued oceanography for almost 100 years, and has been one of the major obstacles to understanding the ocean circulation.

In practice, most investigators assumed values for b, c by asserting that there was some depth, z_0 (or equivalently, a temperature or pressure surface), where $u(x, y, z = z_0(x, y)) = v(x, y, z = z_0(x, y)) = 0$, implying $b(x, y) = c(x, y) = 0$ and then proceeded to discuss the implications of the resulting flow field. z_0 was commonly referred to as the "level-of-no-motion." This approach is the classical "dynamical method." (The t-dependence is generally omitted from here on.) Although there is definite evidence that at great depths the flow becomes comparatively small compared to its near-surface values, unhappily there is neither quantitative evidence nor theory suggesting that a true depth of no flow, even one that might be a complicated function, $z_0(x, y)$, exists anywhere. Even very small velocities, when integrated over large depths, can produce substantial water, and property, transports.

On the other hand, from Eqs. (6.10)–(6.13), it *is* possible to find an expression for the three components of velocity, as (Needler, 1985)

$$\rho(x, y, z)[u, v, w] = g\frac{\hat{\mathbf{k}} \cdot (\nabla\rho \times \nabla q)}{\nabla(f\partial q/\partial z) \cdot (\nabla\rho \times \nabla q)}\nabla\rho \times \nabla q, \quad q = f(y)\frac{\partial\rho}{\partial z} \tag{6.19}$$

Alternate derivations can be found in Pedlosky, 1987; and in Wunsch, 1996. Here ∇ is the three-dimensional gradient operator, and $\hat{\mathbf{k}}$ is the vertical unit normal vertical vector. Equation (6.19) shows that, up to the approximations implicit in the equations used, *a knowledge of the density field alone is adequate to completely determine the absolute oceanic flow field*. In practice, expression (6.19) is never used – for two reasons: (1) it involves the third derivative of the density field, in the element $\nabla(f\partial q/\partial z)$, rendering the calculation hopelessly noisy and, (2) exploration of the sea by ships most commonly takes place along linear tracks, precluding the calculation of density gradients normal to the track.

Because inverse methods were first introduced into oceanography to deal with the determination of absolute geostrophic velocities, we now review that application. Fundamentally, it involves using the same equations that lead to (6.19), but in an approximate, linearized, form that is less noise sensitive than the exact expression, and that will reduce to the canonical $\mathbf{Ex} + \mathbf{n} = \mathbf{y}$.

Consider the transport of properties by a geostrophic flow. Let the concentration of a scalar property (temperature, carbon, oxygen, etc.) be given by $C(x, y, z)$ per unit mass (suppressing t). Then if the geostrophic flow is known, the integrated flux in the meridional direction of C between $x = x_1$ and $x = x_2$ lying between two depths $z_1(x)$ and $z_2(x)$ is

$$V_c(y) \equiv \int_{x_1}^{x_2}\int_{z_1(x)}^{z_2(x)} \rho C(x, y, z)[v_R(x, y, z) + b(x, y)]\,\mathrm{d}z\mathrm{d}x, \tag{6.20}$$

which is made up of a part owing to the thermal wind and a part owing to the unknown reference-level velocity. The dependence upon z_0 is now implicit. A corresponding expression exists for the flux in the zonal direction. From here on, we will use v, b to denote the two velocities normal to the section, irrespective of the true direction of flow or of the x, y coordinates, as the Cartesian approximation does not distinguish between x, y in the thermal wind. When the property is mass itself, $C = 1$. Transport calculations are of very great importance both because they underlie all large-scale property conservation statements, but also because the overall movement of properties, C, which can include temperature (enthalpy), freshwater, oxygen, and carbon, among other quantities, are determinants of biological productivity and of climate. If the term involving $b(x, y)$ in Eq. (6.20) is arbitrarily set to zero, then an error occurs in the computation of V_c. Suppose $b \approx 1$ mm/s, a small oceanographic velocity, and that $C = 1$, so that the transport of mass is being calculated. Then in a 5000 m deep ocean, with b extending over 3000 km, its mass flux contribution is

$$\int_{x_1}^{x_2} \int_{z_1(x)}^{z_2(x)} \rho b(x, y = y_c)\, \mathrm{d}z\mathrm{d}x \approx 3000 \text{ km} \times 5000 \text{ m} \times 10^3 \text{ kg/m}^3 \times 10^{-3} \text{ m/s}$$
$$= 15 \times 10^9 \text{ kg/s},$$

(y_c is constant) or about 50% of the mass transport of the Gulf Stream near Florida. So, as asserted above, small velocities at depth can generate unacceptable errors in transport calculations.

How can one determine the missing integration constants, using the two equations omitted in the classical dynamical method, but without having to resort to using third derivatives of the calculated density field? (The example shown in Fig. 1.5 described the seemingly artificial problem of determining an absolute flow field when only its vertical derivatives were available. For many decades it was the central problem of physical oceanography – through equations (6.15) and (6.16).)

It is useful first to slightly complicate this relatively simple story in two ways:

1. The direct action of the wind blowing on the ocean drives a local flow, usually called the "Ekman transport."[4] This flow is confined to roughly the upper 100 m of the ocean, and does not produce any readily measured influence on the density field – it is thus invisible to observers who only measure temperature and salinity on board a ship. In practice, Ekman transports are estimated from climatological wind fields provided by meteorologists. At any given location, define the Ekman mass flux as F_E, in the direction normal to the section or station pair. Any property C is advected by the Ekman layer, as $F_C = \bar{C}_E(x, y, z_E)F_E$, where $\bar{C}_E$ is the mean of C over the Ekman layer depth. We will write the horizontally integrated Ekman flux of C as $\overline{F_C} = \overline{C_E F_E}$. This contribution has to be accounted for in any flux or conservation statements.
2. The ocean is stably stratified in density, so that any vertical motion, w, carries fluid of one density into a region of lower $(w > 0)$, or higher $(w < 0)$ density. If the stratification

is to be maintained in the presence of a time average w, then the fluid with density anomalous compared to its surroundings must be mixed with fluid of a compensating density so as to maintain the steady state. This process of mixing is often represented as a pseudo-diffusive mass flux in the vertical direction using an empirical coefficient, K_v, multiplying the vertical density gradient, so that the vertical density flux becomes approximately

$$w\rho - K_{\mathrm{v}}\frac{\partial \rho}{\partial z}, \tag{6.21}$$

and Eq. (6.10) is modified to

$$u\frac{\partial \rho}{\partial x} + v\frac{\partial \rho}{\partial y} + w\frac{\partial \rho}{\partial z} - \frac{\partial}{\partial z}\left(K_v \frac{\partial \rho}{\partial z}\right) = 0. \tag{6.22}$$

It is common to define z as normal to the surfaces of constant density, rather than as strictly vertical. For many purposes, the near-vertical oceanic stratification renders the difference immaterial. Sometimes it is either not necessary, or it is infeasible, to separate the effects of w and K_v, so a combined variable w^* is defined so that (6.22) becomes

$$u\frac{\partial \rho}{\partial x} + v\frac{\partial \rho}{\partial y} + w^*\frac{\partial \rho}{\partial z} = 0,$$

where

$$w^* = \left[w\frac{\partial \rho}{\partial z} - \frac{\partial}{\partial z}\left(K_v \frac{\partial \rho}{\partial z}\right)\right] \Big/ \frac{\partial \rho}{\partial z},$$

and analogously for any property C.

6.2.3 Integral version

The equations above are in differential form. In practical use, an integral representation is preferred (although an exception is outlined later). Note that the Navier–Stokes equations are commonly derived from the integral form, letting the volumes involved become differentially small; we now reverse that process. Consider Eq. (6.20), the flux across a line, when written generally,

$$V_C = \iint \boldsymbol{\rho}\mathbf{C}\mathbf{v}\cdot\hat{\mathbf{n}}\mathrm{d}z\mathrm{d}s + \overline{F_C}, \tag{6.23}$$

where the Ekman flux appears only if the vertical integration extends to the sea surface. s is now being used as the horizontal coordinate in place of either x or y and is just a horizontal line element.

Consider any closed volume of ocean, made up of horizontal line segments (Fig. 6.1). Flux of C in and out involves the flow through vertical boundaries plus anything entering or leaving across horizontal ones. Invoking Gauss's and Stokes's

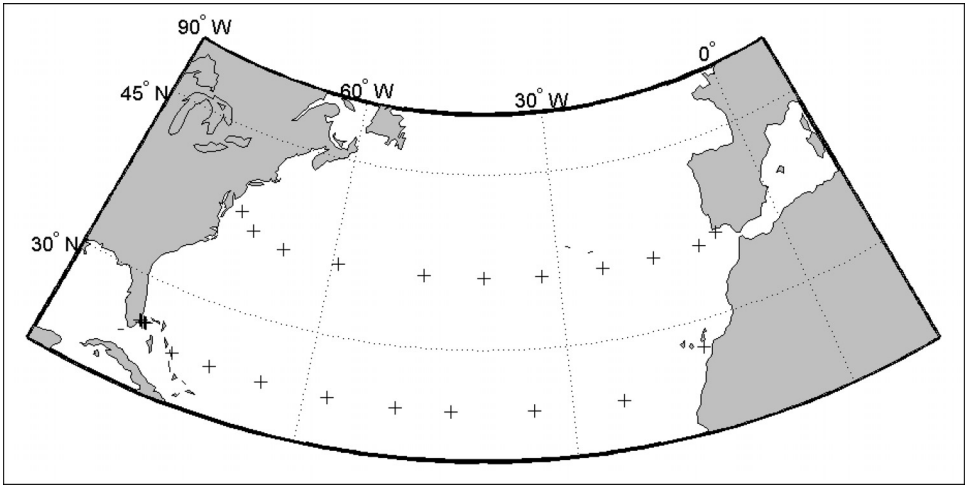

Figure 6.1 Station positions used in prototypical box inversion. There are six stations (five pairs) in the Florida Straits, not visible at this map resolution. A total of 23 station pairs defines the flow into the box, and there is a w_i^* at each of nine isopycnal interfaces. Nominal section names of "Florida Straits," 24° N, and 36° N are used to label the groups of stations. Another box lying between 36° N and the northern boundary of the North Atlantic is also defined, but is not used here.

theorems, Eq. (6.13) becomes

$$\iint \boldsymbol{\rho C v}\cdot\hat{\mathbf{n}}\mathrm{d}A - \iint \left(w\rho C - K_v\frac{\partial \rho C}{\partial z}\right)\Big|_{z_{i+1}} \mathrm{d}A + \iint \left(w\rho C - K_v\frac{\partial \rho C}{\partial z}\right)\Big|_{z_i} \mathrm{d}A + \sum_i \overline{F_C}^{(i)} = \iiint m_C \mathrm{d}V, \tag{6.24}$$

where $z_i\,(x,\,y)$ are bounding surfaces, in the vertical coordinate; $\hat{\mathbf{n}}$ is the unit normal to lateral bounding surfaces, e.g., the zonal or meridional sections; $\mathrm{d}V$ is the volume differential; and $\sum_i \overline{F_C}^{(i)}$ is the sum of the Ekman fluxes (if the top layer is included), over the different lateral segments. We will make the convention here that inwardly directed flows are positive (the reverse of the usual convention). In the combined form, Eq. (6.24) becomes

$$\underbrace{\iint \boldsymbol{\rho C v}\cdot\hat{\mathbf{n}}\mathrm{d}A}_{\textit{horiz advection}} - \underbrace{\iint w^*\rho C\big|_{z_{i+1}}\mathrm{d}A}_{\textit{vert. advection}} + \underbrace{\iint w^*\rho C\big|_{z_i}\mathrm{d}A}_{\textit{vert. advection}} + \underbrace{\sum_i \overline{F_C}^{(i)}}_{\textit{Ekman flux}} = \underbrace{\iiint m_C \mathrm{d}V}_{\textit{mass source}}. \tag{6.25}$$

These equations are algebraic statements that what flows in, must flow out, except for that amount of C produced or consumed within the volume by the source/sink m_C.

6.2.4 Discrete version

Although the equations have been written, as is conventional, in continuous form, they are solved almost universally using computers, and are necessarily discretized. In the thermal wind equations (6.17) and (6.18), density is computed from the equation of state as $\rho(x_j, y_j, z_k, t)$ at horizontal positions, x_j, y_j, at vertical positions z_k and times t (typically about every 2 m in the vertical, 30–50 km in the horizontal, and separated laterally by times of a few hours). The measurement "stations" are used in pairs for computing the horizontal derivatives $\Delta\rho/\Delta x$, $\Delta\rho/\Delta y$, written here as $\Delta\rho/\Delta s$. Integrals in Eqs. (6.18), (6.20) and (6.25) are calculated from discrete approximations to the integrals (often with a trapezoidal rule), the summations running upward and downward, starting from $z_i = z_0$, the reference depth. (Depth is most commonly measured in pressure units, but that is a technical detail.) Thus an estimate from the thermal wind of the relative velocity perpendicular to any pair of stations is:

$$\rho v_R(x_j, y_j, z_q) = \rho v_R(j, q) \approx \frac{g}{f} \sum_{k=0}^{q} \frac{\Delta\rho(j, k)}{\Delta x(j)} \Delta z_k. \tag{6.26}$$

Here $\Delta\rho(j, k) = \rho(x_{j+1}, y_{j+1,} z_k) - \rho(x_j, y_{j,} z_k)$, or some similar horizontal difference, and it is assumed that x_j lies along the section (t is being suppressed). Note the substitution $x_j \to j$, etc.

The conservation equation for mass (6.25), when integrated (summed) from top-to-bottom, becomes

$$V_C \approx \sum_{j\in J} \sum_{q} \rho_j(q) C(j, q)[v_R(j, q) + b_j]\Delta a(j, q) + \overline{F_C}, \tag{6.27}$$

which is obtained from (6.26). The notation $j \in J$ is used to denote the summation over the station pairs lying along the section in question. $\Delta a(j, q)$ is the area occupied in the section between depths z_q, z_{q+1}, over pair separation $\Delta s(j)$. That is, $\Delta a(j, q) = \Delta s(j)(z_{q+1} - z_q)$. An approximation sign has been used in Eq. (6.27) both because of the numerical errors incurred in the discretization, but also acknowledging the reality that we are using an approximate physics (of which the assumption of a steady state is the most stringent), and that because ρ and F_C are obtained from measurements, they are necessarily somewhat inaccurate. In recognition of the inaccuracy, and because equalities are far easier to work with, re-write the equation as

$$V_C = \sum_{j\in J} \sum_{q} \rho(j, q) C(j, q)[v_R(j, q) + b_j]\Delta a(j, q) + \overline{F_C} + n_1, \tag{6.28}$$

where n_1 is the noise.

Using w^*, the net flux of C into a closed region becomes

$$\sum_{j\in J}\sum_{q}\rho(j,q)C(j,q)\delta(j)\Delta a(j,q)[v_R(j,q)+b_j] \tag{6.29}$$
$$-\rho_{k+1}C_{k+1}w^*_{k+1}A_{k+1}+\rho_k w^*_k C_k A_k+\sum_i \overline{F_C}^{(i)}+n_2=m_C,$$

where n_2 represents whatever noise is required to render the equation an equality. Here $\delta(j)=\pm 1$ depending upon whether a positive velocity represents a net flow into or out of the volume. A_k is the horizontal area of density ρ_k multiplying the pseudo-vertical velocity w^*_k, and C_k is the corresponding horizontal average property on the surface. q is the index in the vertical used to sum the properties between interfaces $k, k+1$. As before, the Ekman fluxes only appear if the top layer(s) is included in the particular equation. m_C now represents any volume integrated source or sink. So, for mass, it would represent (in the top layer) any net evaporation or precipitation; for oxygen it would involve photosynthetic production, gas exchange with the atmosphere, and oxidation at depth.

Equations such as (6.28) and (6.29) represent constraints on the flow field, and thus upon the unknown integration constants b_j, and unknown vertical exchanges w^*_i. The solution to the venerable problem of determining the geostrophic flow in the ocean is reduced to writing down enough such constraints that one can make useful inferences about the b_j, w^*_i. In practice, the number of knowns, b_j, can be very large, even thousands. It should be clear, however, defining $\mathbf{x}^{\mathrm{T}}=[[b_j]^{\mathrm{T}},[w^*_j]^{\mathrm{T}}]$, $\mathbf{n}=[n_j]$, or $\mathbf{x}^{\mathrm{T}}=[[b_j]^{\mathrm{T}},[w_j]^{\mathrm{T}},[K_{vj}]^{\mathrm{T}}]$, that they all are in the conventional form

$$\mathbf{E}\mathbf{x}+\mathbf{n}=\mathbf{y}, \tag{6.30}$$

and can be addressed by the methods of Chapters 2 and 3.

This discussion is far from exhaustive. Within the context of linear models, one can incorporate complex structures describing whatever physics, chemistry, or biology that is reasonably believed to depict the observed fields. But if the model (6.30) fails to represent important governing physics, etc., one may be building in errors that no mathematical machinery can overcome.

6.2.5 A specific example

Consider an intermediate scale problem. Three hydrographic sections in the North Atlantic (Fig. 6.1) are used to define a closed volume of ocean within which various fluid properties are likely conserved. Along the lines, each pair of stations defines the relative velocity. The original trans-Atlantic sections (Roemmich and Wunsch, 1985) had a total of 215 stations, but for reasons of discussion and display, the number is here reduced to 25 (6 in the Florida Straits, 8 from the Bahama Bank to

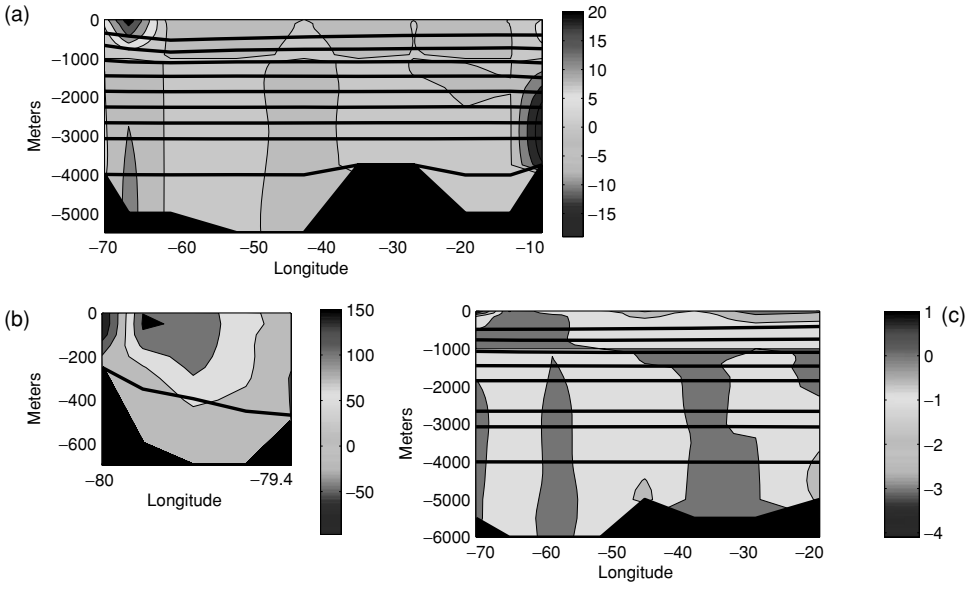

Figure 6.2 Geostrophic velocity (colors, in cm/s) relative to a 1000-decibar reference level, or the bottom, whichever is shallower, and isopycnal surfaces (thick lines) used to define ten layers in the constraints. Part (a) is for 36° N, (b) for the Florida Straits, and (c) for 24° N east of the Florida Straits. Levels-of-no-motion corresponding to the initial calculation are visible at 1000 m in the deep sections, but lie at the bottom in the Florida Straits. Note the greatly varying longitude, depth, and velocity scales. (See color figs.)

Africa along nominally 24° N, and 11 along the nominal 36° N section) producing 23 usable pairs for computing the thermal wind. The water column is divided into 10 layers bounded by isopycnals and/or the top and bottom. (The box model on p. 111 is a simplified analogue of this one.)

For the present primarily pedagogical purposes, the reference level z_0 was fixed at 1000 m (actually measured as a pressure of 1000 decibars, where a decibar is the hydrostatic pressure exerted by one meter of sea water) and which shows up in a zero-line along the sections shown in Fig. 6.2. In the Florida Straits section, which is shallower than 1000 m, z_0 was defined to be at the bottom. In practice, one would try to choose an initial reference level to reflect whatever knowledge one had of the circulation prior to the computation. In particular, note that there is a strong tendency for the sense of the geostrophic flow to reverse across the reference level. It would be sensible, should one have reason to believe that such a reversal occurred in practice, to place the reference level at the transition depth. If the data being used prove too noisy to add useful information, one would find that $\tilde{\mathbf{x}} = \mathbf{0}$, and the resulting best estimate of the ocean would revert to the statement

that it was geostrophic with no flow at $z = z_0$. (We repeat: no such depth following any simple rule exists – the ancient idea that there is some approximately constant depth where $v = 0$ is unsupported by any observations or theory; it is a convenient numerical device for defining and calculating a relative velocity. In the absence of information, however, $v = 0$ may be the best available estimate.)

The spatial resolution being used here is so poor that no sensible oceanographer would expect the result to be very realistic. For example, the Gulf Stream velocities visible in Fig. 6.2 are generally much too low, as are the temperatures being assigned there. Nonetheless, the orders of magnitude are roughly correct and the aim is to be demonstrative rather than to be definitive.

The procedure is to write as many equations as we can involving the unknown b_i, w_j^*, representing whatever is thought true about the field, with some estimate of how accurate the constraints are. One reasonable equation asserts that in a steady state, the total mass flowing into the volume must vanish, up to the errors present; evaporation and precipitation are too small to matter in such a small area. Estimates derived from the windfield suggest that there is an Ekman flow to the south across 36° N of about 3×10^9 kg/s, and about 6.5×10^9 kg/s to the north across the 24° N line (ignoring the very small Ekman contribution in the Florida Straits).[5]

A net Ekman flux into the box of $(3 + 6.5) \times 10^9$ kg/s $= 9.5 \times 10^9$ kg/s can be sustained in a steady state only if it is exported by the geostrophic flow. We can write an equation insisting that the total geostrophic flow across 36° N has to be (approximately) equal and opposite to the southward-going Ekman flux across that line, and that the sum of the mass fluxes across the Florida Straits and 24° N has to balance the 6.5×10^9 kg/s driven northward by the wind in the surface layer. Thus total mass balance provides one equation, and the three individual section flux constraints provide three more; note, however, that these equations are redundant, in that the sum of the net flux equations (taking account of the sign of the flux) must sum to the total mass balance equation. No particular harm is done by carrying redundant equations, and there is some gain in obtaining solution diagnostics, as we shall see.

Many years of direct measurement in the Florida Current (the name for the Gulf Stream in that region), suggest that its time average mass flux is approximately 31×10^9 kg/s to the north. Using the bottom reference level, the relative velocity produces only 22×10^9 kg/s to the north, and some non-zero b_j are expected in any solution producing a transport of about 31×10^9 kg/s there.

We now have four equations (only three of which are independent) in 32 unknowns. A number of possibilities exist for additional constraints. Oceanographers have evidence that the rate of mixing of fluid across surfaces of constant density (isopycnals) tends to be quantitatively small.[6] In other words, fluid entering the ocean volume defined in Fig. 6.1 between two different densities, $\rho_i \leq \rho \leq \rho_{i+1}$,

can be expected to be leaving. Given, however, that some exchange (mixing) of different density types can occur, we may wish to account for it. Using the reduced form, Eq. (6.29), add, with ten layers and ten equations,

$$\sum_j \sum_q \rho(j,q) b_j \delta_j \Delta a(j,q) - \rho_i w_i^* A_i + \rho_{i+1} w_{i+1}^* A_{i+1} + n_i = -\sum_j \sum_q \rho(j,q) v_R(j,q) \delta(j) \Delta a(j,q). \tag{6.31}$$

All unknowns, b_j, w_i^*, n_i have been placed on the left-hand side. In the top layer, the upper boundary is at the seasurface, and the corresponding w_i^* is zero; similarly the lowest layer lower boundary is at the seafloor and $w_i^* = 0$. For the moment, Ekman fluxes are being deliberately omitted, to demonstrate the appearance of model error. Evaporation and precipitation are again ignored as being very small.

With ten layers, we obtain ten additional equations of the form (6.31). In addition to the new equations, we have introduced nine new unknowns w_i^* (the number of interior isopycnals defining ten layers) exactly equal to the maximum number of independent new equations (whether all the layer equations are really independent needs to be determined), as well as an additional nine new noise unknowns, n_i. The top-to-bottom sum of these ten layers must be the same as the equation previously written for total mass conservation. In that sum, all of the w_i^* drop out. The main reason for using isopycnals as the layer boundaries, as opposed, e.g., to constant depths, is to render $w_i^* = 0$ as a reasonable starting solution – that is, one that would be acceptable if the new equations do not produce useful new information. The number of independent equations thus cannot exceed 12. That adding new equations generates twice as many new unknowns, w_i^*, n_i, is nonetheless advantageous, follows from the ability to specify information about the new unknowns in the form of their statistics (specifically their covariances).

Note that in Eq. (6.31) and elsewhere, the elements of the coefficient matrix, $\mathbf{E}$, involve observed quantities (e.g., $\rho(j,q)$, $\Delta a(j,q)$), and thus the elements of $\mathbf{E}$ contain errors of observation, $\Delta\mathbf{E}$. The system of equations, rigorously, instead of being of the canonical form (6.30), should really be written as

$$(\mathbf{E} + \Delta\mathbf{E})\,\mathbf{x} + \mathbf{n} = \mathbf{y}.$$

Neglect of $\Delta\mathbf{E}\mathbf{x}$ relative to $\mathbf{E}\mathbf{x}$, represents a linearization of the system, whose validity must always be a concern. This linearization of the problem is the price being paid to avoid using the high spatial derivatives appearing in the exact expression Eq. (6.19). We here neglect the non-linear term, assuming its influence to be negligible. Let us now analyze the existing 14 equations in 32 unknowns.

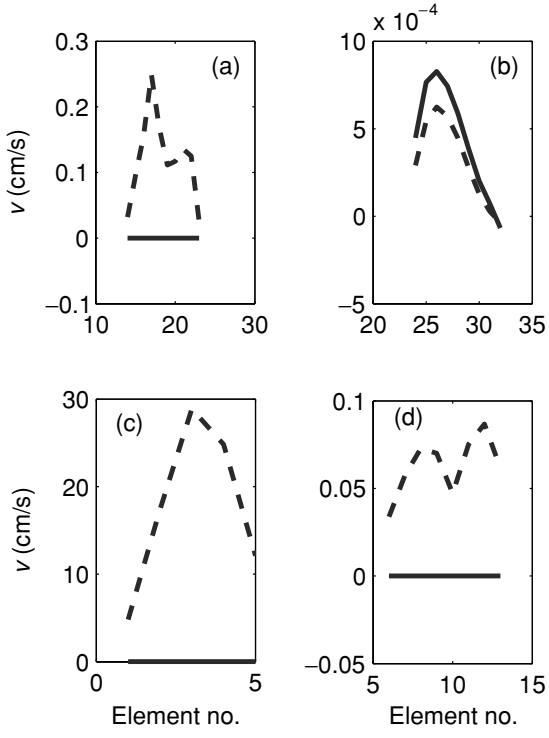

Figure 6.3 The solution to the box model at ranks $K = 9$ (solid line), 12 (dashed line), corrresponding to Fig. 6.4. (a) Results shown for $x_i = b_i$ in the 36° N section, (c) and (d) are the corresponding values for the Florida Straits and 24° N sections, respectively. The values of w_i^* are displayed in (b). Note the weaker values of w_i^* for $K = 12$ relative to $K = 9$. Abcissae is the value of i in x_i.

6.2.6 Solution by SVD

Proceeding to use least-squares, by invoking the singular value decomposition on the equations written down in "raw" (unscaled) form, two solutions, for ranks $K = 9, 12$ are displayed in Fig. 6.3. The singular values are displayed in Fig. 6.4. Two of the values are extremely small (not precisely zero, but so small relative to the others that a reasonable inference is that they represent roundoff errors). Thus the rank of this system is at best $K = 12$ as anticipated above. When plotted on a linear scale (also in Fig. 6.4), it is seen that an additional three singular values are significantly smaller than the others, suggesting some information in the equations which is likely relatively noise sensitive.

To proceed, form the data resolution matrices, $\mathbf{T}_u(K)$ for $K = 9, 12$, whose diagonals are depicted in Fig. 6.4. With $K = 9$, the total mass transport equations are completely unresolved – a perhaps surprising result. (The figure caption lists the order of equations.) If one examines the corresponding $\mathbf{T}_v(9)$, one finds that *all*

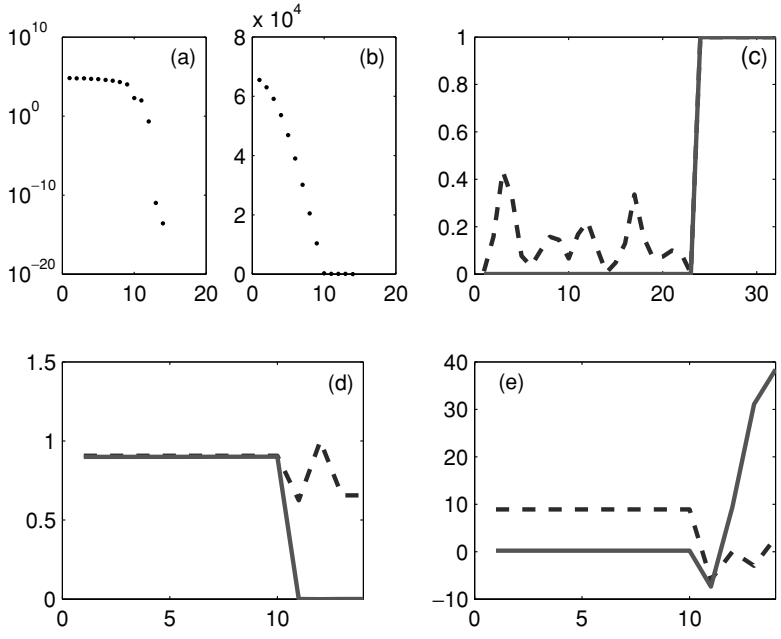

Figure 6.4 (a) and (b) Singular values, λ_i, shown as both logarithmic and linear values for the simple mass balance equations defined by the stations shown in Fig. 6.1. Two λ_i are zero, corresponding to the known redundancy built in, and three are distinctly smaller than the others. (c) $\mathbf{T}_v$ at rank 9 (solid) and at rank 12 (dashed). At rank 9, only the interior layer equations are active, and only the w_i^* are resolved. (d) The diagonal elements of $\mathbf{T}_u$ at ranks 9 (solid) and 12 (dashed). Large residuals (e) are left in the top-to-bottom flux equations when $K = 9$ (the corresponding $\mathbf{T}_u$ shows that they are inactive). At rank 12, there is partial resolution of the b_i, and all equations are active in the solution. The $K = 12$ residuals have been multiplied by 10 for visibility. Residual units are 10^9 kg/s. Note that the first ten elements are all positive – a symptom of the inherent contradiction left present by the omission of the Ekman flux in the layer equations. Order of equations: (1)–(10) are mass balance in each of the individual layers; (11) is total box mass balance (sum of Eqs. (1)–(10)); (12) sets the Florida Straits transport; (13) specifies the 24° N Ekman flux; (14) sets 36° N Ekman flux.

of the w_i^* are fully resolved, and *none* of the reference level velocities b_i is resolved at all, consistent with the zero values for the b_i with $K = 9$. Why should this be? Examination of the columns of $\mathbf{E}$ shows that the interface areas, A_k, multiplying the w_k^* are of order 3×10^4 times larger than the vertical areas multiplying the b_i. Or, alternatively, the column norms of $\mathbf{E}$ corresponding to the w_i^* are much larger than for the b_i. Recalling that a singular vector solution solves the least-squares problem of minimizing the solution norm for the smallest possible residual norm, it is unsurprising that the system would seek to make the w_i^* finite relative to the b_i, because small values of w_k^* have a greatly amplified effect on the residuals.

The rank 9 solution is then found to be $\tilde{b}_i \approx 0$, and the $\tilde{w}_i^*$ as shown in Fig. 6.4(b), corresponding to an upwelling throughout the water column. Although the w_i^* are somewhat large, the real reason for rejecting this solution is the behavior of the residuals. Strong violation of the overall mass balance constraints is occurring – vertical velocities alone cannot produce the import and export of fluid required to balance the overall mass budget, and the net flux constraint through the Florida Straits.

To invoke the constraints on overall (top-to-bottom) mass balance, increase the rank to $K = 12$, with diagonals of $\mathbf{T}_u$ shown in Fig. 6.4 demonstrating the new importance of the equations for overall balance. The rank 12 solution (Fig. 6.3) and its residuals (Fig. 6.4e) are also displayed. Now the residuals in all layers are 0.9×10^9 kg/s, but the top to bottom mass imbalance is -0.6×10^9 kg/s and the two zonal flux integrals fail to balance by $\pm 0.3 \times 10^9$ kg/s.

In looking at the solution, we see that the reference level velocities in the Florida Straits (bottom velocities) are of order 10–20 cm/s, while elsewhere, they range from 0.01–0.1 cm/s. The $\tilde{w}_i^*$ are all positive, increasing to a mid-depth maximum from 1×10^{-4} cm/s at the lowest interface to 7×10^{-4} cm/s in the middle of the water column.

This solution might be an acceptable one, but it is to some degree an accident of the various row and column norms appearing in matrix $\mathbf{E}$. For example, some of the layers are thinner than others, and they are given less weight in the solution than thicker ones. Whether this outcome is desirable depends upon what the investigator thinks the appropriate weighting is. The $\tilde{w}_k^*$ values are perhaps a bit large by conventional standards, but before attempting to control them, note the main reason for solution rejection: a contradiction has been left in the system (for demonstration purposes). The total top-to-bottom mass flux was required to vanish so that the geostrophic flow exported the net incoming Ekman flux. But in the individual layer equations, the Ekman flux was omitted altogether. Because the sum of the ten layer equations should be the same as the total top-to-bottom mass balance, there is a contradiction. The present solution has resolved this contradiction by leaving mass residuals in each of the layers – corresponding to a weak, unexplained, mass source in them. It is this mass source, when summed vertically, that permits the geostrophic outflow to balance the Ekman inflow.

The system has apportioned the erroneous ageostrophic flow over all layers – it had no information to the contrary. That there is a systematic error is shown to the user by the fact that at $K = 12$, *all of the layer imbalances have the same sign* (Fig. 6.4(e)) – if the residuals were pure noise, they should have a much more random character. This example demonstrates a truism of such methods: most of the information about solution acceptability or shortcomings is obtained from the residuals. To account for the systematic error, one can "inform" the

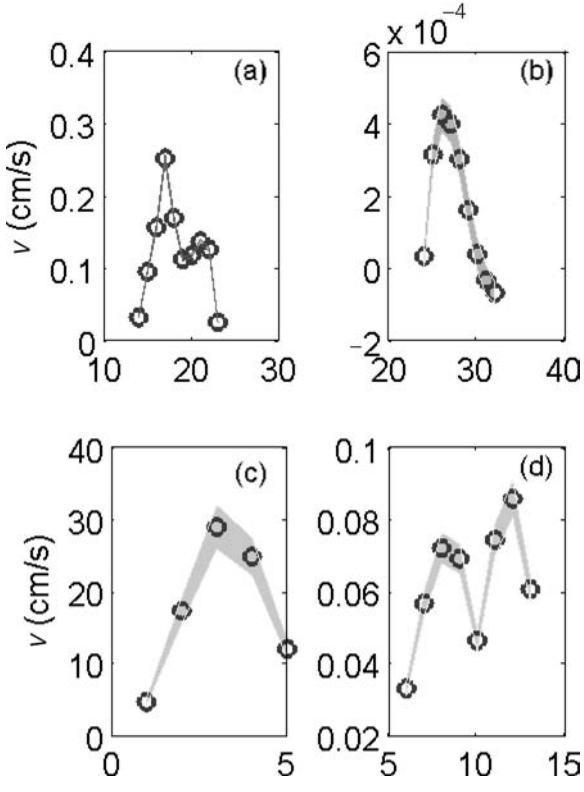

Figure 6.5 Inverse solution by SVD, now consistently accounting for the Ekman flux, for $K = 12$. As before, but now the very small standard error is also displayed (shading) as determined from the diagonal elements of $\mathbf{C}$. The $K = 9$ solution is not detectably changed from that shown in Fig. 6.4. (a) 36° N values of $\tilde{b}_i$; (b) $\tilde{w}_i^*$, (c) and (d) $\tilde{b}_i$ for the Florida Straits and 24° N sections, respectively.

system, that the Ekman flux is probably confined to the uppermost layer by requiring that the net geostrophic outflow there should be equal and opposite to the Ekman inflow.

When that is done, the $K = 12$ solution changes very slightly overall (Fig. 6.5), but the layer mass residuals are very much smaller and fluctuating in sign (Fig. 6.6). The main point here is that the slightly subtle error in the equations (the model), is detected because the residuals do not behave as expected. In the present case, in the consistent system, the residuals are now too small – they are inconsistent with the prior estimates of their magnitude. In a more realistic situation, this outcome would be cause for suspecting a further error. Here, the explanation is immediate: the y_i were artificially constructed so that all equations are now fully consistent and there are no errors present other than roundoff noise.

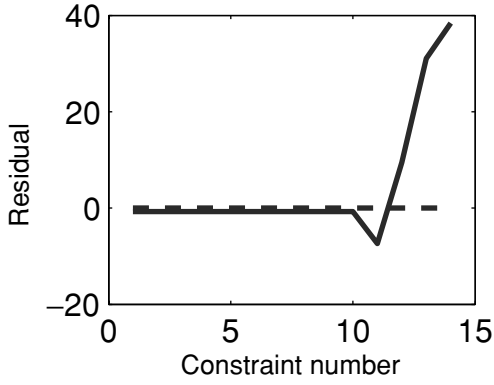

Figure 6.6 Residuals for the consistent mass conservation, at $K = 9$ (solid), and $K = 12$ (dashed). The latter are vanishingly small by construction of the artificial "observations."

The SVD solution permits a full description of the relationship of the equations and the structure of the solution. Figure 6.7 shows the singular vectors of the mass-conserving system. Consider the first term in the SVD solution:

$$\tilde{\mathbf{x}} = \frac{\left(\mathbf{u}_1^{\mathrm{T}}\mathbf{y}\right)}{\lambda_1}\mathbf{v}_1.$$

The orthonormal structure, proportional to $\mathbf{u}_1$ in $\mathbf{y}$, produces an orthonormal structure $\mathbf{v}_1$ in the solution. These two vectors are displayed in Fig. 6.7. The dot product of $\mathbf{u}_1$ with $\mathbf{y}$, forms the successive differences on the right-side of the equations, that is, approximately, $-y_1/2 + y_2 - y_3 + \cdots + y_{10}/2$, with some extra emphasis on the equations for layers at intermediate depths in the water column. The corresponding structure, $\mathbf{v}_1$, is approximately zero for all of the b_i, but is non-zero in the w_i^*. Because $w_{1,10}^*$ each appears in only one equation, whereas all the others appear in two of them – the flow into one layer being the flow out of its neighbor – the two end layer equations are given roughly $1/2$ the weight of the interior ones. When dotted with $\mathbf{x}$, $\mathbf{v}_1$ produces, approximately, the sum $(-w_1^* + w_2^* - w_3^* + \cdots)$ again with some extra weight assigned in the middle of the water column. The strongest information present in the set of equations concerns the differences of the vertical transfers, which are proportional to $-w_1^* + w_2^* - w_3^* + \cdots$, that is the vertical convergences, layer-by-layer in the vertical. The second most important information available concerns a different set of differences of the w_i^*. The first nine $\mathbf{u}_i$, $\mathbf{v}_i$ pairs shown in Fig. 6.7 pertain to the w_i^* – evidently information about the unknown b_i is weak in these equations, as we already knew. The $\mathbf{u}_{10}$, $\mathbf{v}_{10}$ pair involving the equations for total mass, and the two meridional flux equations, evidently carry the most important information about the b_i: the (weighted) differences of the flows

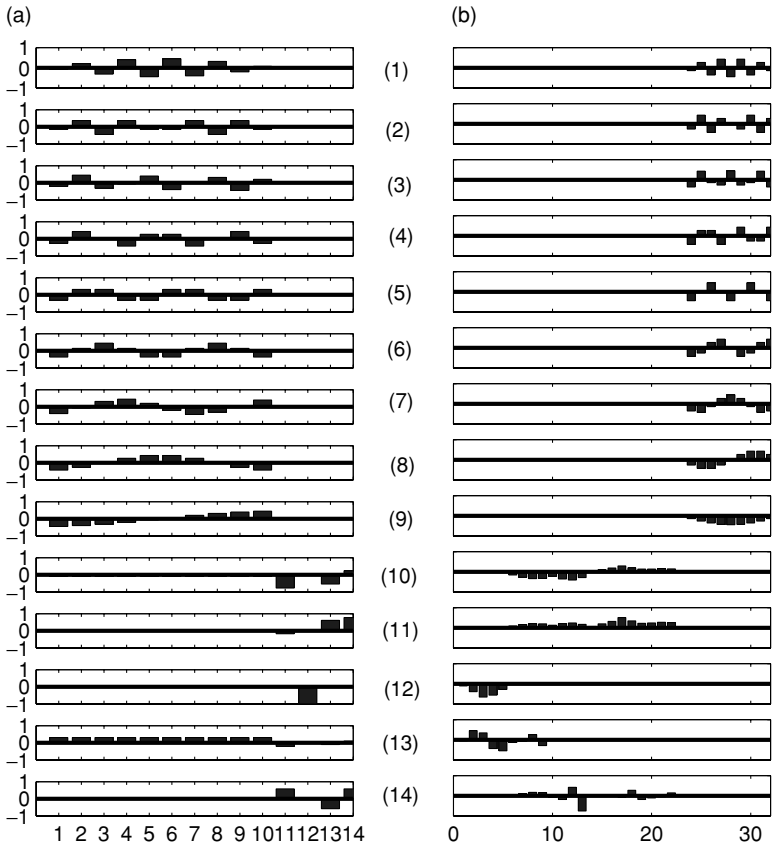

Figure 6.7 (a) First 14 of the $\mathbf{u}_i$, $\mathbf{v}_i$ pairs. The first ten equations describe layer-by-layer mass balance, Eq. (11) is top-to-bottom mass balance (redundantly with the sum of Eqs. (1)–(10); Eq. (12) enforces the observed mass flux through the Florida Straits, and Eqs. (13) and (14) impose a top-to-bottom geostrophic flow equal and opposite the 24° N and 36° N Ekman fluxes. (b) The first five unknowns are the Florida Straits reference level velocities; (6)–(13) are the reference level velocities in the 24° N section, and (13)–(33) are in the 36° N section. As discussed in the text, for $\mathbf{u}_1$, $\mathbf{v}_1$, successive differences of the layer equations resolve sums of w_i^*. Note that $\mathbf{u}_{12}$, which brings in only the Florida Straits mass flux constraint, corresponds to a weighted mean of the bottom velocities there. $\mathbf{u}_{13}$, when dotted with the equations, asserts that the sum of the ten-layer equations, with overall box mass balance plus and minus the 24 and 36° N mass balances, should add to zero (they are redundant). The 13th and 14th $\mathbf{u}_i$, $\mathbf{v}_i$ are in the nullspace. A dot product with $\mathbf{u}_{14}$ asserts that the 11th equation (box mass balance), is redundant with the difference of the 24 and 36° N mass balances, which we know to be true. The corresponding $\mathbf{v}_{13,14}$ are linear combinations of b_i about which there is no information.

across 24 and 26° N. Pair 12 is particularly simple: it involves only the equation that sets the Florida Straits mass flux to 31×10^9 kg/s; only the Florida Straits velocities appear in it.

Controlling the solution

The solutions shown are determined in large part by the various row and column norms appearing in $\mathbf{E}$. For example, the very large horizontal areas multiplying w_i^* give them high resolution, and values at depth that some might regard as too high. Without entering into a debate as to the reality of the outcome, we can nonetheless gain some control over the solution – *to the extent that it does not actually conflict with the equations themselves.*

Following the principles outlined in Chapter 2, column-normalize by the square root of the column lengths – putting all elements on an equal footing. A reasonable estimate of the rank is still $K = 12$. A solution (not shown) to this column-normalized form does *not* produce equal elements – the equations do not permit it. For example, in the Florida Straits, the horizontal velocities remain of order 20 cm/s, and the w_i^* are O(10^{-7} cm/s). Indeed, no solution of uniform magnitude could simultaneously satisfy the Florida Straits flux conditions, and the interior mass balances.

In the spirit of least-squares then, we remain free to impose any prior weights that we wish. Having column-normalized, we can impose variances on the x_i. The b_i variances in the Florida Straits will be estimated as 100 $(\text{cm/s})^2$, outside that region, they are about 1 (cm/s), and $(10^{-5}$ cm/s$)^2$ for the w_i^*. These values are meant to roughly reflect prior knowledge. Thus,

$$\mathbf{R}_{xx} = \text{diag}([100\,(\text{cm/s})^2, \ldots, 1\,(\text{cm/s}), \ldots, (10^{-5}\text{cm/s})^2]). \tag{6.32}$$

Now let us try to gain control over the residuals left in each equation. A plausible analysis suggests the Florida Straits mass flux of 31×10^9 kg/s is accurate to about $\pm 2 \times 10^9$ kg/s, and that the various Ekman fluxes are accurate to about $\pm 1 \times 10^9$ kg/s. Total mass balance is required to $\pm 0.5 \times 10^9$ kg/s, and in the individual layers to $\pm 1 \times 10^9$ kg/s. No information is available about the covariances of the errors among the equations (not strictly true). Because of the different layer thicknesses being used in the constraints, the equations have very different contributions to the solution for any finite rank. We thus opt to first divide each equation by its corresponding row norm, and then weight it by the square root of

$$\mathbf{R}_{nn} = \text{diag}\{1\ 1\ 1\ 1\ 1\ 1\ 1\ 1\ 1\ 1\ 1/(0.5)^2\ 1/2^2\ 1\ 1\}, \tag{6.33}$$

in units of $(10^9$ kg/s$)^{-2}$. Note that we are making the a-priori inference that the noise estimates apply to the row-normalized equations; determining whether this inference is the best one becomes a discussion of the specifics of noise in oceanographic

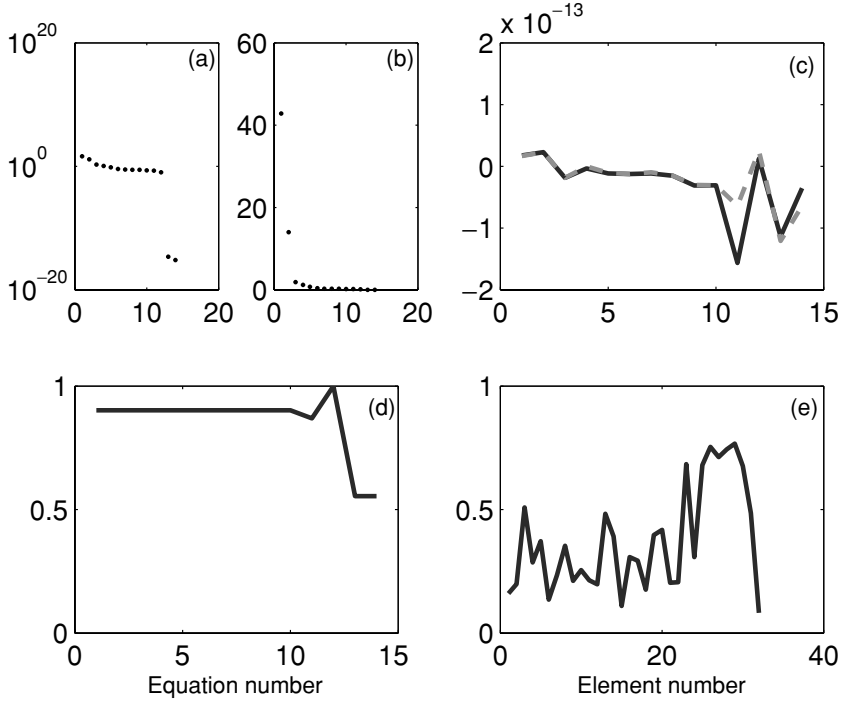

Figure 6.8 Singular values on a logarithmic (a) and linear (b) scale, for the row and column normalized mass-conserving system; (c) the non-dimensional (solid) and dimensional residuals (dashed) when $K = 12$; (d) $\mathbf{T}_u$; and (e) $\mathbf{T}_v$ for $K = 12$.

measurements and computation. For the present, it is a reasonable choice. The fully scaled system is then (Eq. (2.131)),

$$\mathbf{E}'\mathbf{x}' + \mathbf{n}' = \mathbf{y}'.$$

Again use the SVD (in the scaled spaces), and take rank $K = 12$ (see Fig. 6.8). Now the resolution of the w_i^* is lower than before, much of the information having gone instead to determining the b_i. Equation (11) (top-to-bottom conservation) is given little weight (but is redundant with the highly weighted sum of Eqs. (1)–(10)). Figure 6.8 displays the singular values, the diagonals at $K = 12$ of $\mathbf{T}_u$, $\mathbf{T}_v$, and the rank 12 residual of the system. The solution itself (in the original, unscaled, space) can be seen in Fig. 6.9 along with its standard errors.

The $K = 12$ rows (or columns) of the dimensional resolution matrices $\mathbf{T}_u$, $\mathbf{T}_v$ are displayed in Fig. 6.10 for this case. The first 12 equations are almost uniformly used in determining the solution. But Eqs. (11) (the overall box mass balance), (13) (the 24° N net mass flux), and (14) (the 36° N net mass flux) are used only in linear combination with each other, which makes sense because they are highly

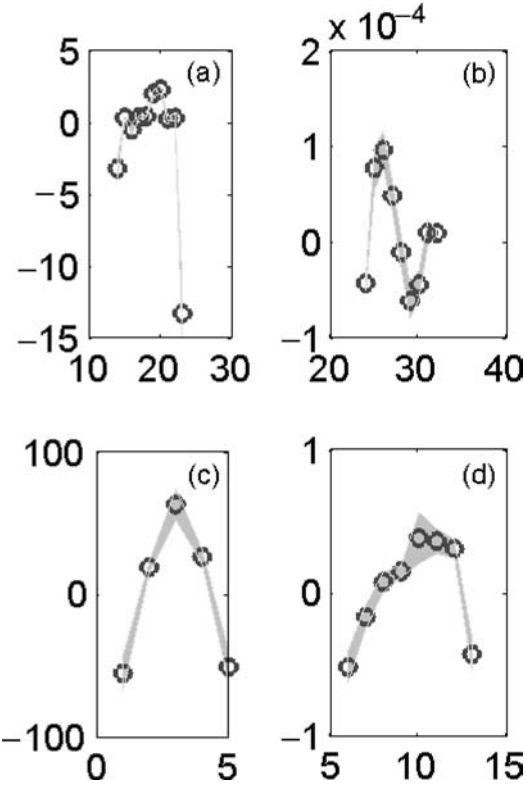

Figure 6.9 Solutions for the row and column normalized mass-conserving system. Graphs (a), (c) and (d) show the $\tilde{b}_i$ in the 36° N, Florida Straits and 24° N sections, respectively, while (d) shows the corresponding w_i^*. Shading is a one-standard-deviation uncertainty estimate.

dependent. Only the equation (12) that fixes the mass transport through the Florida Straits is fully resolved. Otherwise, all equations have some partial projection onto the others, giving rise to dependencies, and produce the two smallest non-zero singular values. The horizontal velocities are resolved in various weighted average groups whose structure can be inferred directly from $\mathbf{T}_v$.

6.2.7 Solution by Gauss–Markov estimate

The great power of the SVD solution is that it provides a nearly exhaustive method to understand exactly why the solution comes out the way it does, permits ordering the equations (data) in terms of importance, and provides estimates of the uncertainty and its structure. As the solution dimension grows, the amount of available information becomes overwhelming, and one may prefer a somewhat more opaque, but nonetheless still very useful, approach. Consider, therefore, the solution by the

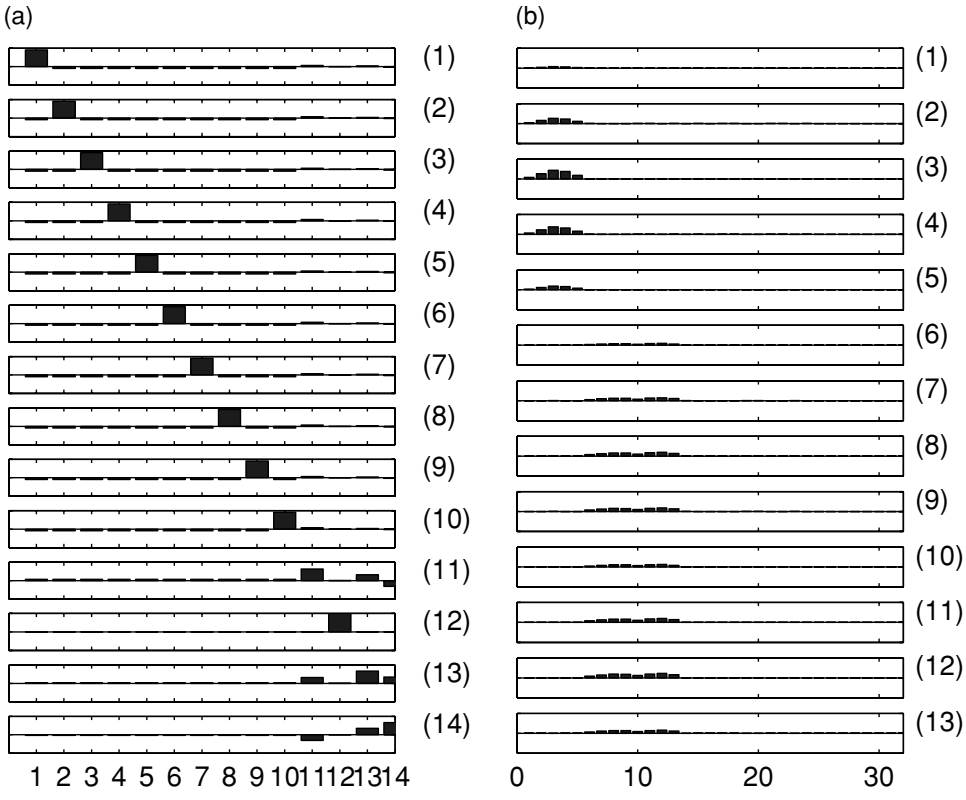

Figure 6.10 (a) The successive rows (or columns) of $\mathbf{T}_u$ for $K = 12$ for the row and column normalized mass-conservation equations. As discussed in the text, Eqs. (11), (13) and (14) show strong dependencies. The order of equations is listed in the caption to Fig. 6.4. (b) The first 13 columns of $\mathbf{T}_v$ (the remaining columns correspond to the w_i^*, which are nearly completely resolved). Full scale in all cases is ± 1. Note that many of the estimated b_i exhibit compact resolution (a local average is determined), as in columns 2–6, where others (e.g., column 8) are determined only in combination with spatially more remote values. None is fully resolved by itself.

Gauss–Markov estimator, Eq. (2.403). In that notation, and consistent with the numbers already used, put $\mathbf{R}_{nn}$ as defined in Eq. (6.33). An a-priori estimate of the solution covariance was taken to be the column weights used above: (Eq. 6.32) for the Florida Straits, open ocean b_i, and w_k^*, respectively. The resulting solution is displayed in Fig. 6.11 along with the formal uncertainty, $\pm\sqrt{\text{diag}\,(\mathbf{P})}$. The solution closely resembles that from the SVD approach. The x_i are seen to be generally consistent with the values in Eq. (6.32), although a few of the w_i^* become somewhat large (but not enough to be truly suspicious). The estimates of $\mathbf{n}$ (not shown) are again, generally too small to be consistent with $\mathbf{R}_{nn}$ – a result that would lead one

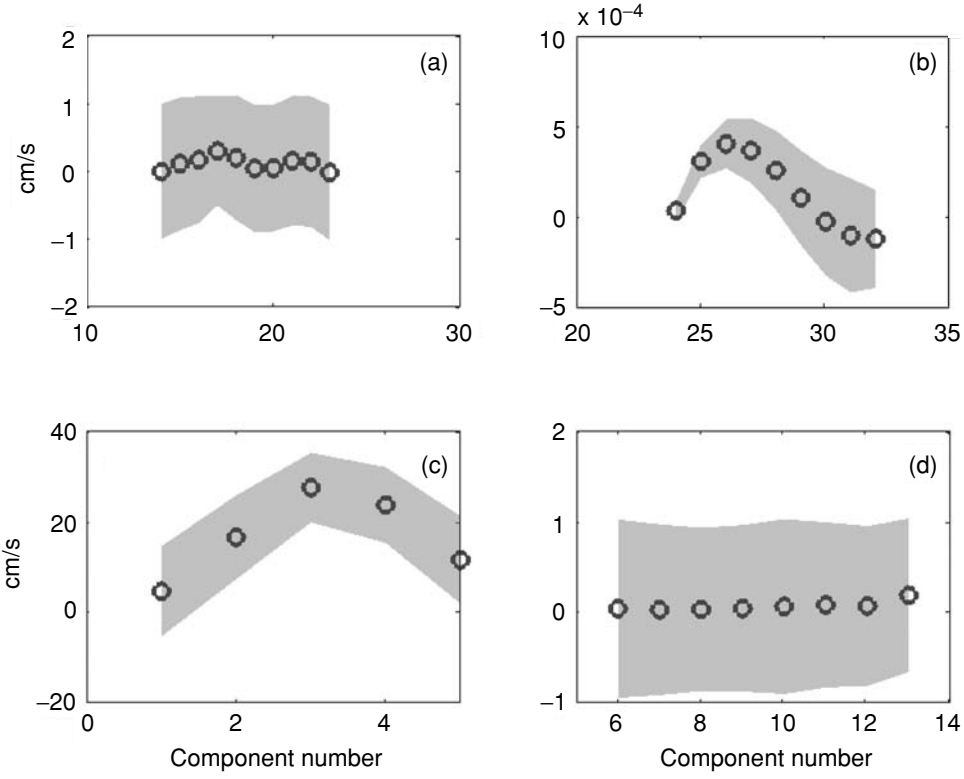

Figure 6.11 Gauss–Markov solution, with standard errors, for the geostrophic box model. Only some of the solution elements are distinguishable from zero within one standard deviation of the error. (a) Results shown for $\tilde{b}_i$ in the 36° N section, (c) Florida Straits, and (d) for 24° N, while (b) is $\tilde{w}_i^*$.

to conclude that the system was inconsistent with the prior covariance, which we know is true because of the artificially low error.

6.2.8 Adding further properties

This approach to estimating b_i, w_k^* can be extended indefinitely by adding conservation requirements on as many properties, C, as have been measured. Among the properties that have been used are salinity, S, silica, and oxygen concentration. The most commonly available property is S, and so let us examine the consequences of using it. Salt is not carried by the atmosphere, and no measurable internal sources or sinks of S exist; in the assumed steady state, however, much salt enters a volume of ocean, so an equivalent amount must exit. Salt conservation equations can be written in the form of (6.25), completely analogous to those already written for mass, including Ekman contributions $\overline{F_S}$, and putting $C = S$, $M_S = 0$. (Note

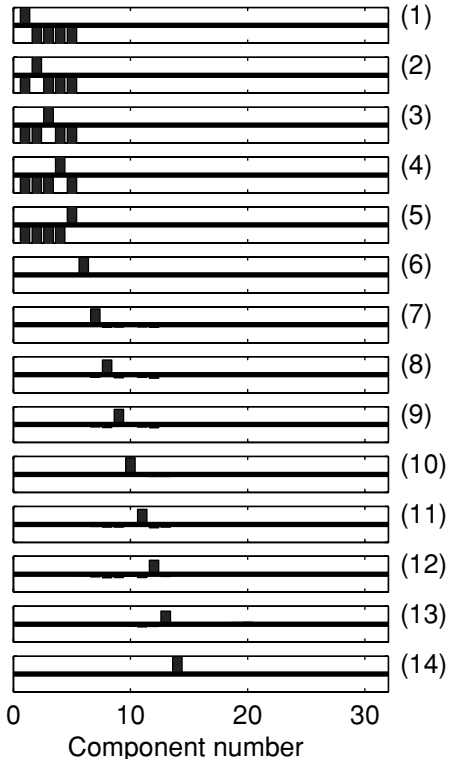

Figure 6.12 First 14 columns (or rows) of the **P** matrix for the solution in Fig. 6.11 corresponding to the $\tilde{b}_i$ elements of the solution, and showing the covariances among the solution elements. All columns are scaled to ± 1, but differ dimensionally by orders of magnitude. Most conspicuous is a strong negative correlation among the errors of the different b_i.

that modern salinity values are dimensionless, and measured on what is called the "practical salinity scale"; despite widespread use, there is no such thing as a "practical salinity unit.") Adding ten equations for salt conservation in the layers to the present system, plus top-to-bottom salt conservation (again redundant), produces 11 additional equations, for a total of 25 equations in the same 32 unknowns. At most ten independent equations have been added. To illustrate, the SVD solution will be used.

Oceanic salinities hardly differ from $S = 35$, so, following the column normalization, row normalize the 13 new equations by 35. The singular values of the new, larger, system are displayed in Fig. 6.13. The new rank could be at most $K = 22$, and indeed there are 22 non-zero singular values, but the range of values is now quite large – over four orders of magnitude. Clearly a choice of the practical rank

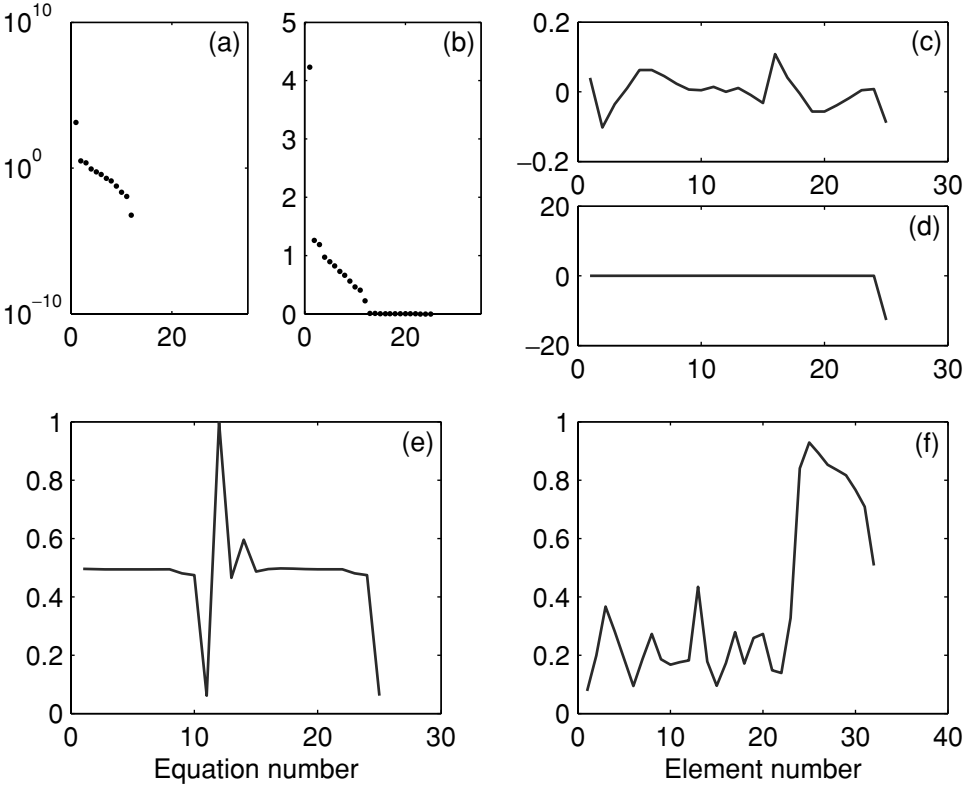

Figure 6.13 Combined mass and salt equations, showing the singular values (a), (b), and the rank 12 diagonals of $\mathbf{T}_u$, $\mathbf{T}_v$ (e), (f). Non-dimensional and dimensional equation residuals are in (c), (d).

depends directly on how small a λ_i can be tolerated. Taking again $K = 12$, the results are shown in Figs. 6.13–6.15.

Why doesn't salt balance prove more useful? If one examines the $\mathbf{u}_i$, $\mathbf{v}_i$ (Fig. 6.15) or the rank 22 resolution matrices (not shown), one sees that the mass and salt equations are seen to have a strong dependency (redundancy). The reason is not difficult to find. The equation of state (Eq. (6.12)) is, in practice, linearizable:

$$\rho \approx \rho_0(1 - \alpha_1 T + \beta_1 S).$$

Thus there is a near linear dependency between ρ (mass) and S. Whether the measurement and model accuracies are sufficient to render the small singular values that result useful is a question that can only be answered in quantitative terms, employing the actual noise levels.

The row normalization by 35, before anything else has been done, renders the resulting values of $C/35 \approx 1$ with little variation. For this reason, some authors

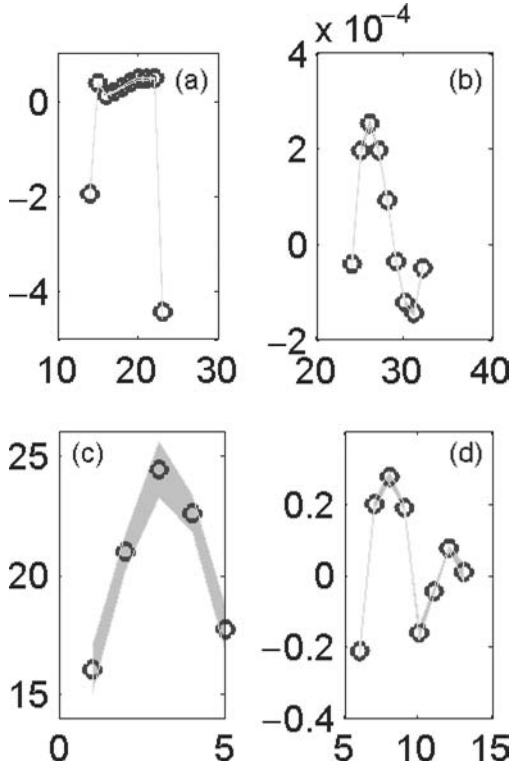

Figure 6.14 SVD solution for the combined mass and salt system. (a) Estimated b_i for the 36° N section, (c), (d) b_i for the Florida Straits and 24° N sections, respectively; (b) shows the estimated w_i^*.

have advocated working instead with the salinity anomaly. Consider a salt balance equation (either flux or overall box conservation), e.g.,

$$\sum_{j\notin J}\sum_{j}\rho(j,q)S(j,q)\delta(j)\Delta a(j,q)[v_R(j,q)+b_j] \qquad (6.34)$$
$$-\rho_{k+1}S_{k+1}w^*_{k+1}A_{k+1}+\rho_k S_k w^*_k A_k+\sum_i \overline{F_S}^{(i)}+n_2=0,$$

and the corresponding mass conservation equation,

$$\sum_{j\in J}\sum_{q}\rho(j,q)\delta(j)\Delta a(j,q)[v_j(j,q)+b_j]-\rho_{k+1}w^*_{k+1}A_{k+1} \qquad (6.35)$$
$$+\rho_k w^*_k A_k+\sum_i \overline{F_E}^{(i)}+n_1=m_\rho.$$

m_ρ has been retained in the mass balance equation to permit a very slight net evaporation or precipitation if the integration extends to the seasurface. $\mathbf{v}$ is the

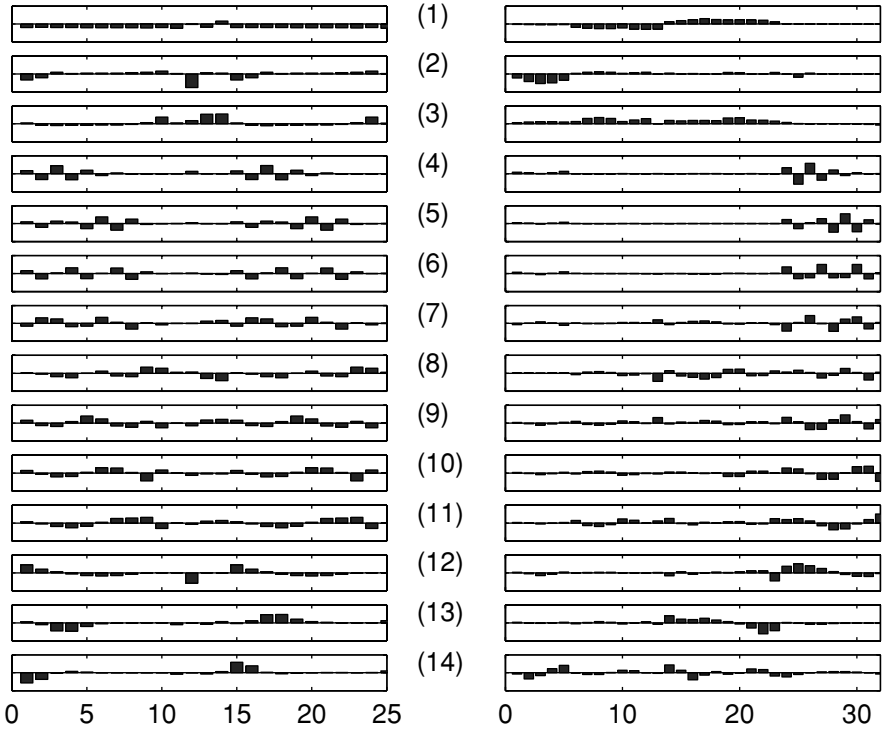

Figure 6.15 First 14 $\mathbf{u}_i$, $\mathbf{v}_i$ for the mass- and salt-conserving system. $\mathbf{u}_1$, $\mathbf{v}_1$ involve a linear combination of all of the equations, that is, primarily determining the b_i in the 24° N and 36° N sections. Elements 1 to 6 in the Florida Straits are determined by a complex combination of equations. Full scale is ± 1 for all.

horizontal velocity. Multiply the second of these equations by $\bar{S}$, and subtract from the first:

$$\sum_{j\notin J}\sum_{q}\rho(j,q)[S(j,q)-\bar{S}]\delta(j)\Delta a(j,q)[v_R(j,q)+b_j] \qquad (6.36)$$
$$-\rho_{k+1}w^*_{k+1}[S_{k+1}-\bar{S}]A_{k+1}+\rho_k w^*_k[S_k-\bar{S}]A_k$$
$$+\sum_i \overline{F_S}^{(i)}-\bar{S}\overline{F_E}^{(i)}+n_2-\bar{S}n_1=\bar{S}m_\rho.$$

This result is a new equation in $S'=S-\bar{S}$. The argument is commonly made that this subtraction improves the numerical conditioning of the system of equations – as the relative variation of S' is much greater than that of S. In practice, this reason is *not* why the system appears to be more useful: modern computers have such large word lengths, and with the accuracies of the input data hardly exceeding five significant figures, ordinary software has no difficulty in exploiting

the small variations in S. The real reason salinity anomaly equations prove useful is quite different; the noise element in the new equation is $n_2 - \bar{S}n_1$, and it is usually assumed that this difference nearly vanishes, producing a strong noise suppression. Although the noise removal will not, in practice, be exact, noise does appear, empirically, to be much reduced. One could obtain the same result by using a non-diagonal $\mathbf{R}_{nn}$, in which a very high correlation was imposed on the noise elements of corresponding mass- and salt-conservation equations. The only reason why that would be preferable is that it makes clearer what is actually going on – it is not the numerical conditioning that matters here, but the assumption about the noise structure. Equation (6.36), when integrated to the surface, cannot normally be used to constrain $\mathbf{x}$, as m_ρ is too poorly known. It is more commonly used to infer m_ρ, from estimates of $\tilde{\mathbf{x}}$ made using the other equations. If the noise does not effectively vanish, the resulting estimate will not be meaningful: m_ρ typically has a magnitude much smaller than any plausible error in the original equations.

6.3 Property fluxes

Mass and salt fluxes have been used in the equations employed to determine $\mathbf{x}$. One of the most important reasons for studying the ocean circulation, however, is the need to compute the fluxes of other scalar properties, physical and chemical, which are central to the climate system. Often, from the estimate of the resulting flow and mixing parameters, one seeks to calculate the fluxes of other important properties that were not necessarily employed as constraints. One might not use them as constraints if, for example, sources and sinks were so uncertain that little useful information would be obtained if realistic errors were assigned. An example would be the top-to-bottom oxygen balance, in the presence of highly uncertain air–sea gas exchange, photosynthesis, and remineralization at depth, all of which might be regarded as essentially unknown. In that case, the m_C appearing on the right-hand side of equations such as Eq. (6.29) would be best obtained by calculating them as residuals of the equations.

If some m_C is so poorly known that one wishes to compute it from $\tilde{\mathbf{x}}$, there are two equivalent approaches. One can include the equation in the set to be solved, but giving it such small weight that it has no influence on the solution. Evaluation of the system residuals then automatically evaluates m_C. The alternative is to omit the equation completely, and then to evaluate it after the fact. In the first approach, the equation system is slightly larger than is strictly necessary, but unless there are many such downweighted constraints, the consequences are slight.

Consider any property transport equation, e.g., for temperature across a line:

$$\tilde{H} = \sum_{j\in J}\sum_{q} \rho(j,q)C(j,q)\delta(j)\Delta a(j,q)\tilde{b}_j \tag{6.37}$$
$$+ \sum_{j\in J}\sum_{q} \rho(j,q)C(j,q)\delta(j)\Delta a(j,q)v_R(j,q) + \overline{F_C}$$
$$= \mathbf{d}^{\mathrm{T}}\tilde{\mathbf{x}} + \sum_{j\in J}\sum_{q} \rho(j,q)C(j,q)\delta(j)\Delta a(j,q)v_R(j,q) + \overline{F_C},$$

$$d_j = \left[\sum_{q} \rho(j,q)C(j,q)\delta(j)\Delta a(j,q)\right].$$

The first term on the right of $\tilde{H}$ is determined from an inversion for b_i^*; the remaining two terms are known. Apart from the numerical estimate of $\tilde{H}$ itself, the most important piece of information is its accuracy. So, for example, estimates of the heat flux across 36° N in the North Atlantic are approximately 1×10^{15} W. For studies of climate and of climate change, one must quantify the expected error in the value. There will be three contributions to that error, from uncertainties in $\tilde{b}_j$, from $v_R(j,m)$, and from F_C. The first error is the easiest to estimate. Suppose one has $\tilde{\mathbf{x}}$, and its uncertainty $\mathbf{P}$. Let the elements of $\tilde{\mathbf{x}}$ corresponding to the b_i be the vector of elements $\mathbf{x}_b$, with corresponding error covariance $\mathbf{P}_b$ (that is, omitting the w_i^*, or other parameters, not appearing in Eq. (6.37)). Then the uncertainty of the flux owing to the errors in $\tilde{b}_i$ is

$$P_{H_1} = \mathbf{d}^{\mathrm{T}}\mathbf{P}_b\mathbf{d}. \tag{6.38}$$

One might attempt then to add the uncertainty owing to the variances of $\overline{F_C}$, and v_{Rj}. The difficulty is that the $\tilde{b}_j$ are determined from $\overline{F_C}$, v_{Rj}, and the errors cannot be considered independently. For this reason, these other errors are usually omitted. A computation of the uncertainty owing to time variations in $\overline{F_C}$, and v_{Rj} is done separately, and is described later on in this chapter.

Consider the heat flux estimated from the Gauss–Markov method used above. Property C is then the temperature, T, times the heat capacity, $h_p = 4 \times 10^3$ J kg^{-1} °C^{-1}. Then, $\tilde{H} = (4.3 \pm 2.2) \times 10^{14}$ W (a number that, owing to the coarse spatial resolution, is too low by about a factor of about 2). The uncertainty was obtained directly from Eq. (6.38). The flux divergence and its error estimate is obtained in the same way, except using instead, the equation for the difference of the 24° and 36° N fluxes. Because of the summation implied by $\mathbf{d}^{\mathrm{T}}\mathbf{P}_b\mathbf{d}$, the error for the flux can be much lower than for individual elements of the velocity field, if error cancellation, owing to spatial correlation structures, can take place. In other circumstances, the errors will amplify through the summation.

An alternative approach is to write $\tilde{\mathbf{x}} = \tilde{\mathbf{x}}_{SVD} + \mathbf{q}$, where $\tilde{\mathbf{x}}_{SVD}$ is the particular SVD solution as defined in Chapter 2, and $\mathbf{q}$ is the nullspace contribution, which is unknown, and which may dominate $\mathbf{P}$, $\mathbf{P}_b$. If the vector $\mathbf{d}$ in Eq. (6.37) is such that $\mathbf{d}^{\mathrm{T}}\mathbf{q} \approx 0$, $\tilde{H} = \mathbf{d}^{\mathrm{T}}\tilde{\mathbf{x}}_{SVD}$, then P_{H_1} will tend to be small. That is, the missing nullspace will have little effect on the heat flux estimate because it is nearly orthogonal to the vector of station heat contents ($\mathbf{d}$). This situation seems to obtain, approximately, over much of the ocean, and thus oceanic heat flux calculations are often more accurate than might have been anticipated, given the large remaining uncertainty in the mass flux owing to its nullspace. Much of that nullspace lies in small spatial scales (eddies).

6.4 Application to real oceanographic problems

The estimation machinery discussed here has been applied in a great variety of physical oceanographic settings, ranging from comparatively small regions involving state vectors $\mathbf{x}$ of modest dimension (tens to hundreds of elements), to global calculations in which $\mathbf{x}$ has thousands of elements. Here we survey some of these calculations, primarily to give the flavor of real problems. It is a truism of most estimation problems that the construction of the model (defining $\mathbf{E}$, $\mathbf{R}_{xx}$, $\mathbf{R}_{nn}$, etc.) and interpreting the result is 90% of the labor, with the actual inversion being comparatively straightforward. Here we omit most of the detail involved in editing real data (temperature, salinity, oxygen, nutrients, etc.) and getting it into a form whereby the station-pair sums in equations like (6.34) and (6.35) can be carried out. The reader is referred to OCIP (Wunsch, 1996) and the references cited there for some of this detail. Software for carrying out practical inversions with real hydrographic data has been developed at a number of oceanographic organizations, and is available over the Internet. But given the ephemeral nature of websites, I will refrain from providing specific sources here.

6.4.1 Regional applications

Numerous applications of these ideas to particular regions exist and only a few will be described. Consider the hydrographic stations in Fig. 6.16 (from Joyce *et al.*, 2001). This single section defines a closed, if complicated, region of ocean to the west, involving much of the western North Atlantic as well as a major part of the Caribbean Sea. In addition to temperature, salinity, and various conventional scalar fields such as nitrate, silicate concentration, the investigators had available direct, if noisy, velocity measurements from a so-called lowered acoustic Doppler current profiler (LADCP). They also had "transient tracer" data in the form of chlorofluorocarbons (CFC-11,12). The density field (computed from temperature,

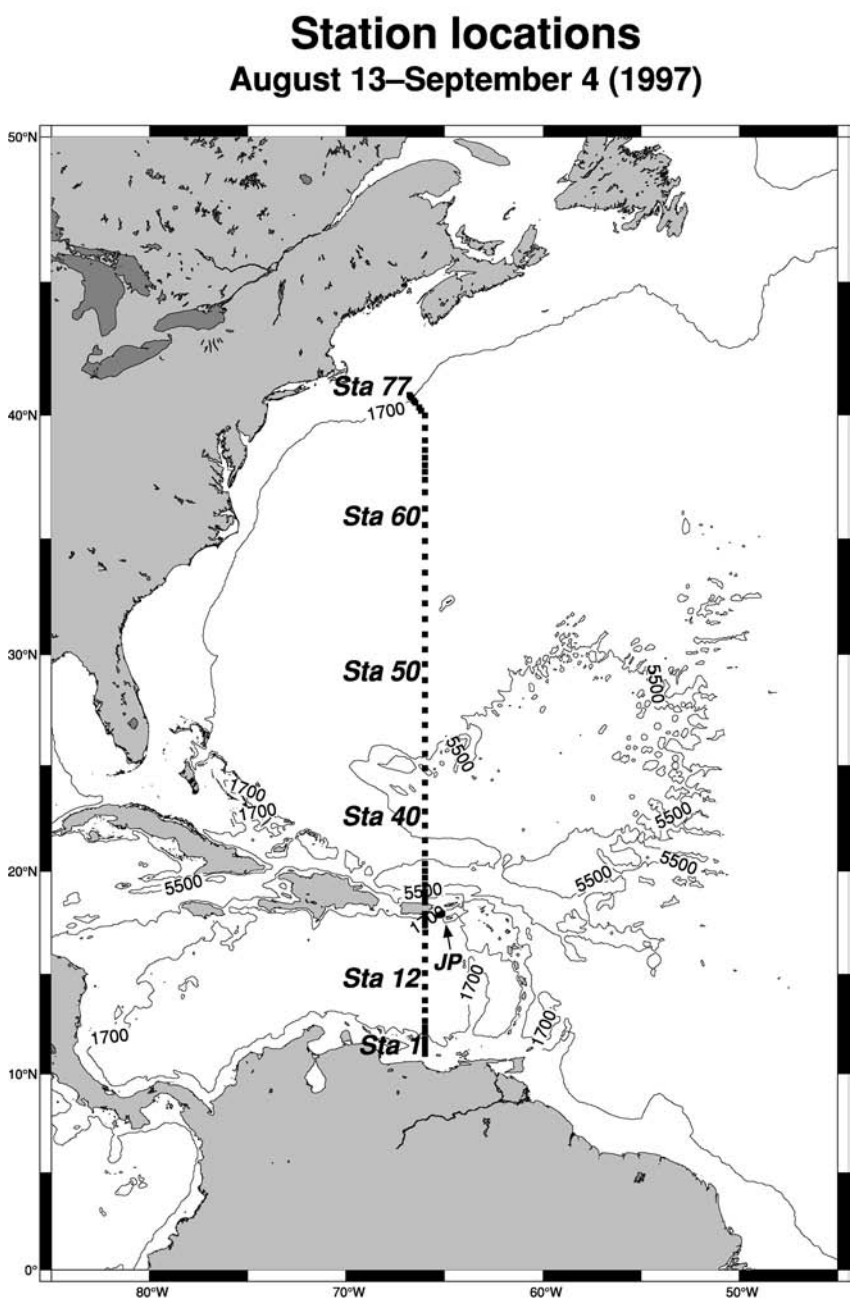

Figure 6.16 Positions of the hydrographic and LADCP measurements taken by Joyce *et al.* (2001). The region to the west of the line represents a closed volume of ocean for which various approximate conservation requirements are written in the form of standard simultaneous linear equations. (Source: Joyce *et al.*, 2001)

salinity, and pressure) and silica concentration are displayed in Figs. 6.17 and 6.18. The goal was to combine all of the data so as to determine the flow field, and the major property fluxes across the line. (Note that one might regard the section as also defining a closed volume consisting of the entire remainder of the world ocean, to which the net inflow/outflow constraints equally well apply. Internal balances involving isopycnal areas would be different, however, and distant outcrops to the surface would be very important.)

Joyce *et al.* (2001) used the LADCP velocities to provide an initial, non-zero, estimate of the reference level velocity; these are most easily employed by adding equations of the form $x_i = v_i$, where the v_i are the LADCP values at the reference level, and the indices i correspond to the reference level velocities, so that $x_i = b_i$. An estimate is made of the accuracy of these new constraints (this procedure is only approximately that used by Joyce *et al.*, 2001). In addition, to mass constraints overall, and in each of the layers (accounting for the Ekman velocity), near-conservation of silica within the system leads to a canonical problem of 44 equations in 72 unknowns. Error variances for the mass flux equations varied from $(2 \times 10^9$ kg/s$)^2$ to $(0.5 \times 10^9$ kg/s$)^2$ for the mass equations; silica equations had error variances ranging from (5–20 kmol/s)^2. In addition, a-priori estimates were made of the reference level variances (see Fig. 6.19). Note that no use was made of vertical exchanges, w^*, and thus any mass transfers across the interfaces will appear in the noise residuals, $\tilde{n}_i$. An inversion was done using the Gauss–Markov estimator; the flow field obtained (see Fig. 6.20) is the best estimate of the combined data sets with the assumptions of geostrophy, a steady state, and an Ekman flux in the surface layer. The resulting flow fields were then used to calculate zonal heat, freshwater, and CFC.

This solution and its employment depicts the general ability to combine data of very different types, to test the adequacy of the model assumptions (residuals are all acceptable), and its application to finding the fluid fluxes of important scalar properties.

The preferred strategy is to write as many constraints on the system as is consistent with prior knowledge, and then to use them to make the best possible estimate of the circulation. Other observation types have been employed by many authors, including direct velocities from mid-depth floats (Mercier *et al.*, 1993); current meters (Matear, 1993); and altimetric measurements of the seasurface height (Martel and Wunsch, 1993a). Gille (1999) used a combination of surface Doppler acoustic measurements of velocity (ADCP), mid-depth floats, and velocities determined from satellite altimeters in addition to the hydrographic data. As always, the only requirement for the use of any kind of data is that there should be an algebraic relationship between the unknowns, x_i, and the observations, and that estimates of the expected errors should be available.

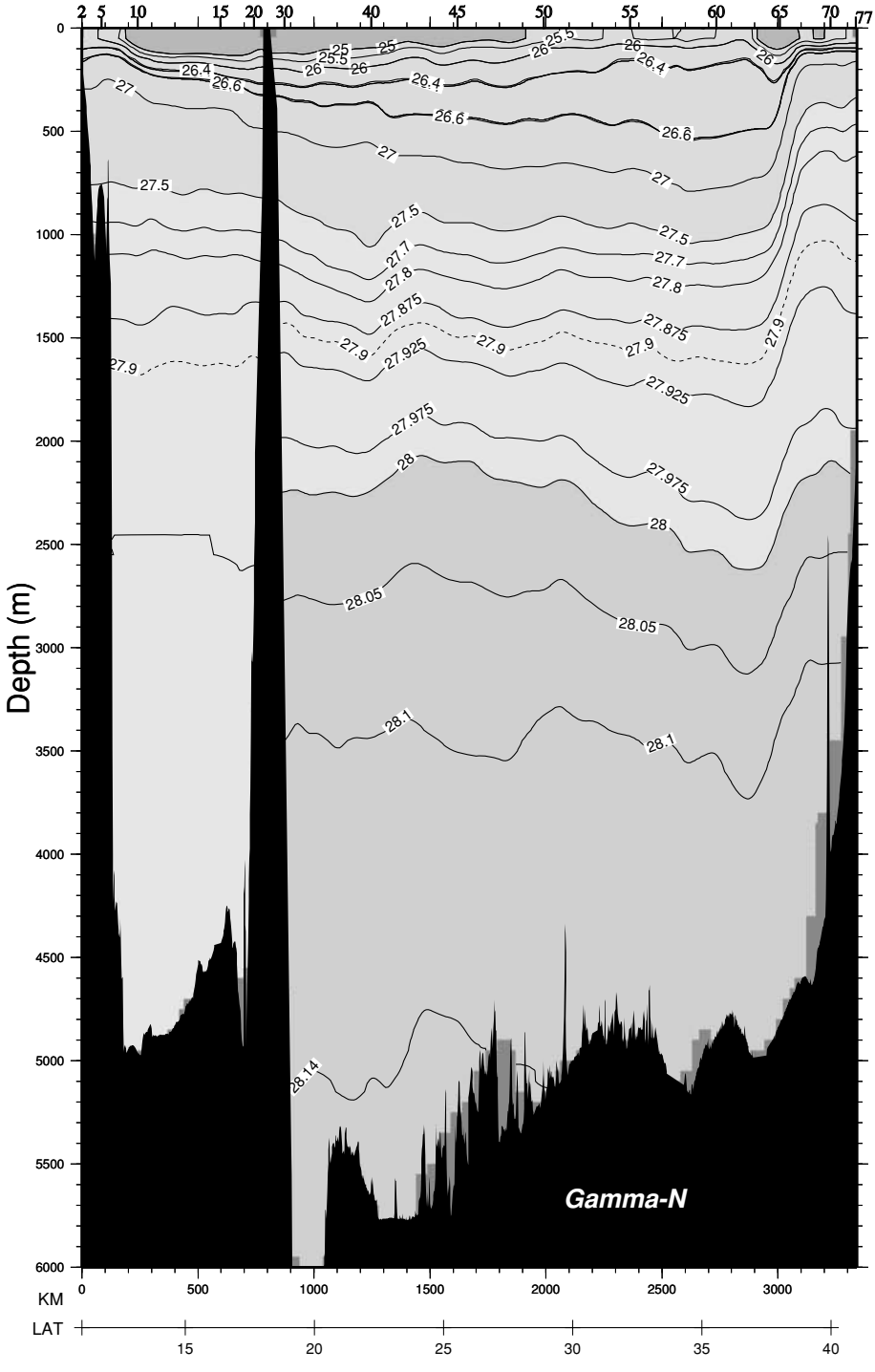

Figure 6.17 Density field constructed from the measurements at the positions in Fig. 6.16. Technically, these contours are of so-called neutral density, but for present purposes they are indistinguishable from the potential density. (See color figs.)

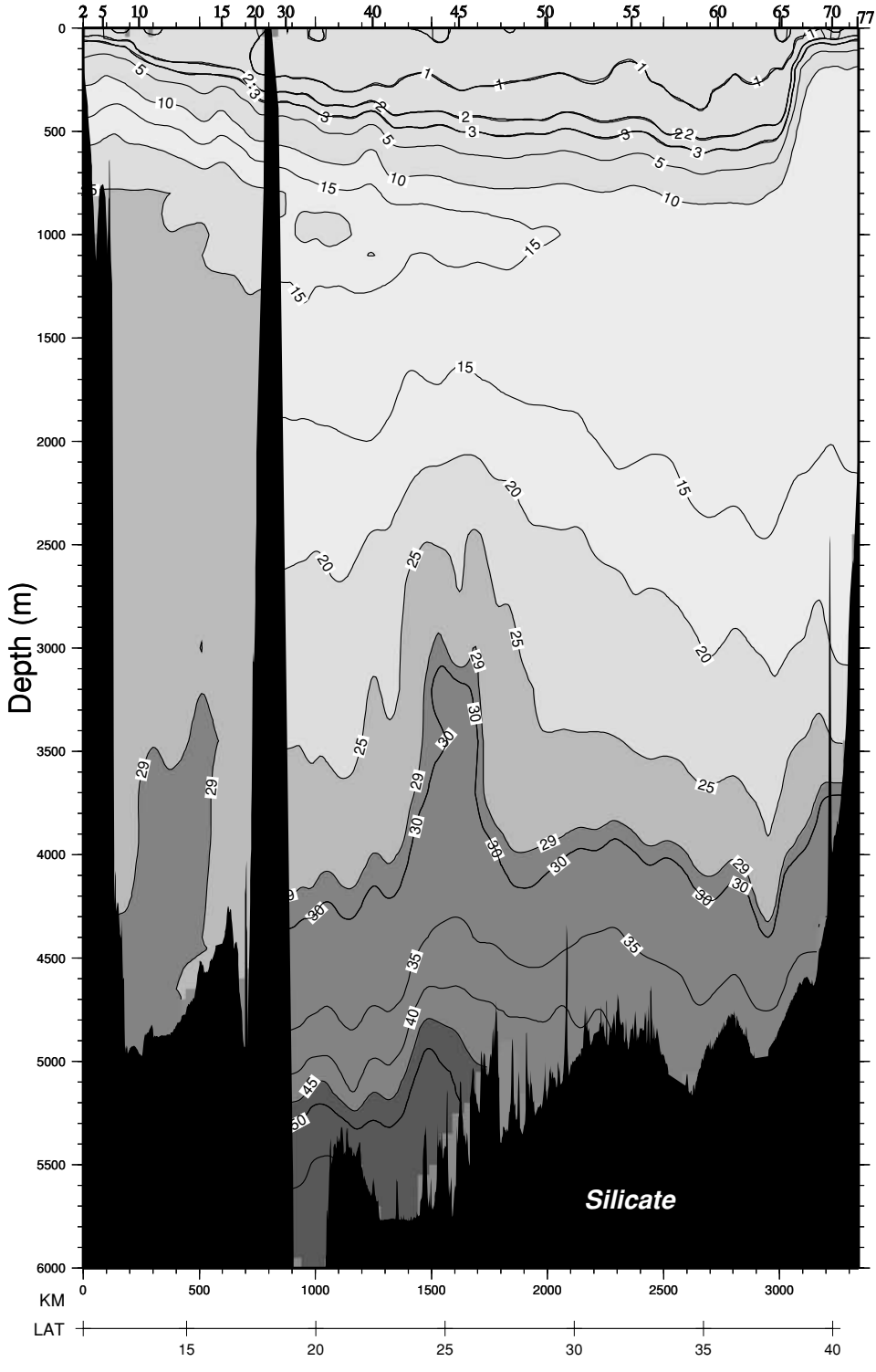

Figure 6.18 Same as Fig. 6.17, except showing the silicate concentration – a passive tracer – in μ moles/kg. (See color figs.)

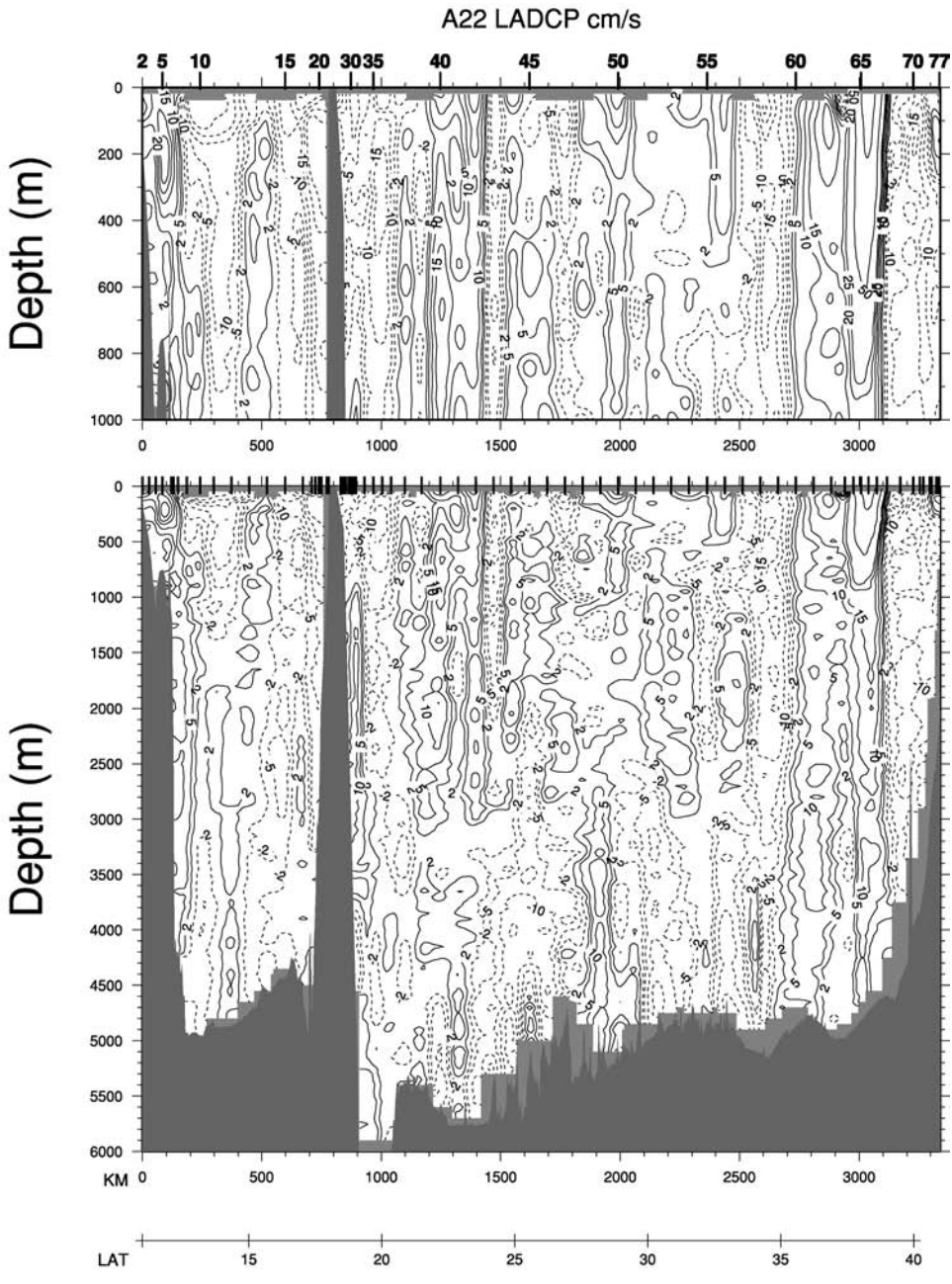

Figure 6.19 Initial velocity field from the hydrographic and LADCP data, as described by Joyce *et al.* (2001). Note the very great noisiness of the data. An expanded version of the upper 1000 m is also shown. (Source: Joyce *et al.*, 2001)

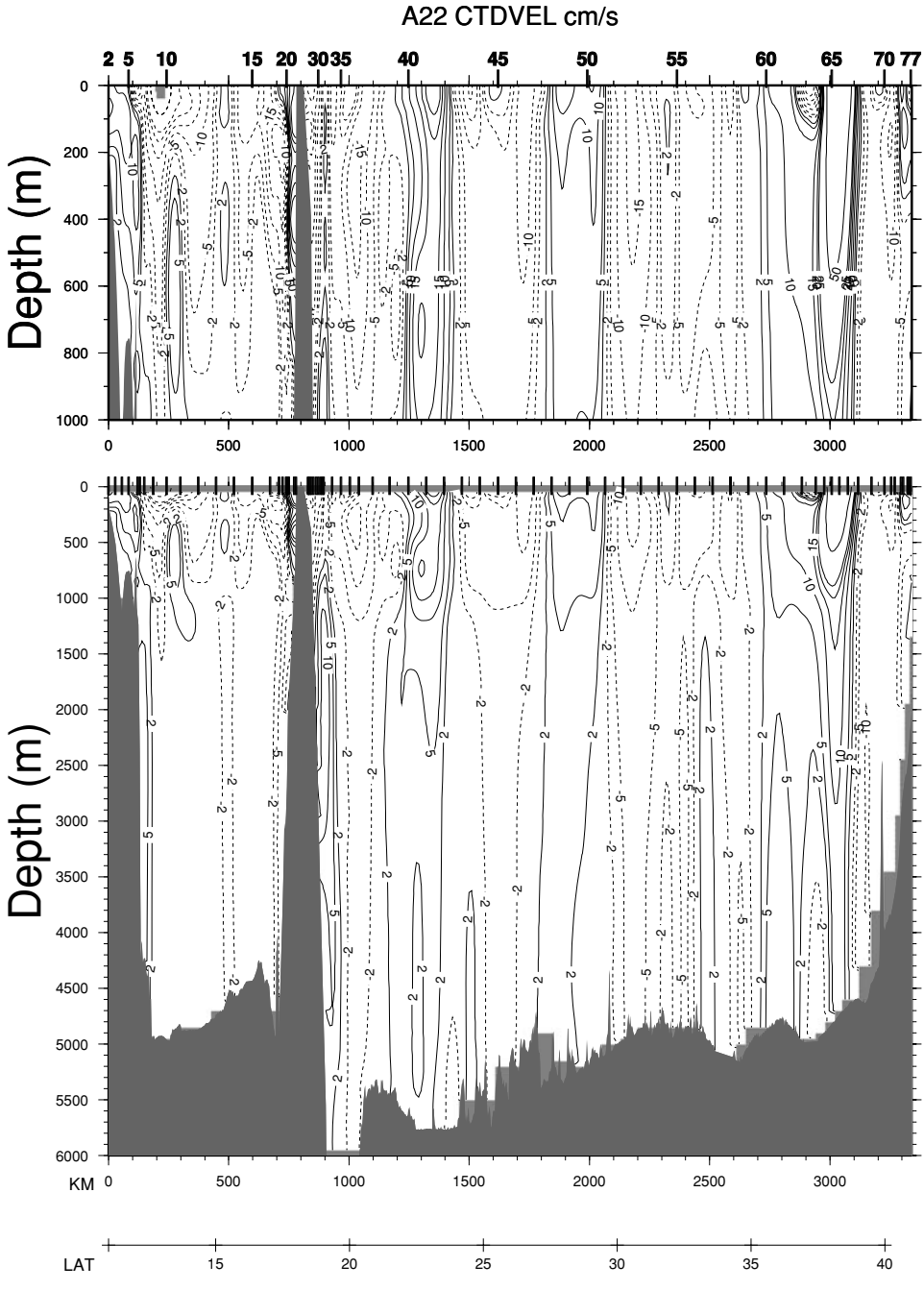

Figure 6.20 Final estimated velocity from the inversion using the constraints of Joyce *et al.* (2001). See their paper for details. Compare to Fig. 6.19, which was the starting point. Note the very strong vertical columnar nature of the estimated flow.

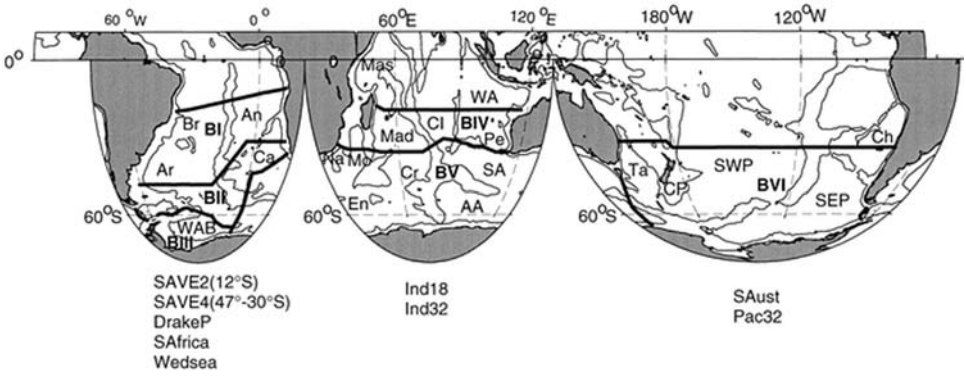

Figure 6.21 Positions of the sections used by Sloyan and Rintoul (2001) to determine the high latitude southern hemisphere oceanic circulation. (Source: Sloyan and Rintoul, 2001)

In another, larger, region Sloyan and Rintoul (2001) used the hydrographic lines depicted in Fig. 6.21. This region is sufficiently large that the results are probably best compared to the global-scale inversions described later. The authors employed 23 layers bounded by neutral surfaces, and the top and bottom. Conservation equations were written for mass, heat, salt, and silica, and a number of section mass transports, as well as a requirement of heat loss over the Weddell Sea, were imposed. A distinguishing feature of this calculation was that Sloyan and Rintoul (2001) permitted the vertical exchange coefficients w^* to be different for different properties (heat, silica, etc.) in contrast to other inversions where they were forced to be identical for all properties. Their solution produced a much more vigorous circulation than is conventionally accepted (e.g., the production rate of Antarctic Bottom Water exceeded 50×10^9 kg/s, which is much larger than conventional wisdom suggests). The extra degrees-of-freedom from the property-variable mixing do not by themselves necessitate a stronger circulation. Rather, one can trace the strong solution back to the choices of a-priori solution and residual values. To the degree that their solution is consistent with all of the imposed information, and in the absence of additional information, it cannot be rejected. One interpretation is that the information employed is inadequate to invalidate a 50×10^9 kg/s bottom water formation rate hypothesis.

Another interesting regional solution is that of Naveira Garabato *et al.* (2003) who focussed on determining the mixing coefficients, K, in the Scotia Sea region of the Southern Ocean, finding remarkably strong abyssal vertical diffusion coefficients.

6.4.2 The columnar result

When inverse methods were initially applied to the ocean circulation problem (Wunsch, 1977, 1978), they elicited a highly skeptical, generally negative, response.

Prominent among the reasons for this reaction was the vertical, or columnar, structures visible in the solutions, e.g., as seen in Fig. 6.20. That the lines of vanishing flow tended to be oriented more vertically, rather than horizontally – as a simple level-of-no-motion would imply – was regarded as strong evidence that the method was producing erroneous results. The level-of-no-motion assumption and related inferences about the ocean, had led to a widespread presumption that the true flows were layer-like. As it gradually became clear that these features were commonplace, and robust, and it was more widely appreciated that there was no rationale for quasi-horizontal levels-of-no-motion, the negative chorus gradually diminished, but has not yet entirely vanished.

It does remain possible that very long time-averages of the solutions would produce time-mean velocities that had a more layered character. A full discussion of this issue more properly belongs in an oceanographic book. But as one piece of evidence, Fig. 6.22 shows the directly measured two-year mean velocity (that is, not inferred from an inverse method) from a moored array of current meters in the western South Pacific Ocean. Note the marked near-vertical orientation of the zero lines. Of course, two years is still an interval short compared to the longest time scales present in the ocean, and a 100-year average might well have a different character, although there is no evidence for it. There would also be serious questions about the interpretation of the time-averaged equations governing such a hypothetical flow – they would not, in general, be the same linear equations we have been using. (The data all lie below 2000 m, but the accompanying hydrography suggests, in fact, that these columns do extend close to the sea surface as in Fig. 6.20.)

6.4.3 Global-scale applications

There have been two attempts at estimating the global ocean circulation with these methods (Macdonald, 1998; Ganachaud, 2003a), and the latter is briefly examined as representative of the state-of-the-art. The sections shown in Fig. 6.23 were used to write approximate conservation equations for the volumes bounded by sections and continents (note that all sections terminate at both ends in shallow water). Properties used as constraints were mass, temperature, salinity, silica, and "PO." The last is a combination of phosphate and oxygen concentrations, "PO" $= 170[PO_4] + [O_2]$, for which biological arguments exist that it should be nearly conservative below the zone of biological productivity (the brackets denote "concentration of"). For present purposes, it is just one more property carried passively by the fluid. Not all properties were required to be conserved top-to-bottom, but some only in interior layers (temperature, "PO"), and silica was conserved only top-to-bottom and not in individual layers. The layers were defined by constant density surfaces (technically, neutral surfaces), and a very large number of auxiliary requirements were written

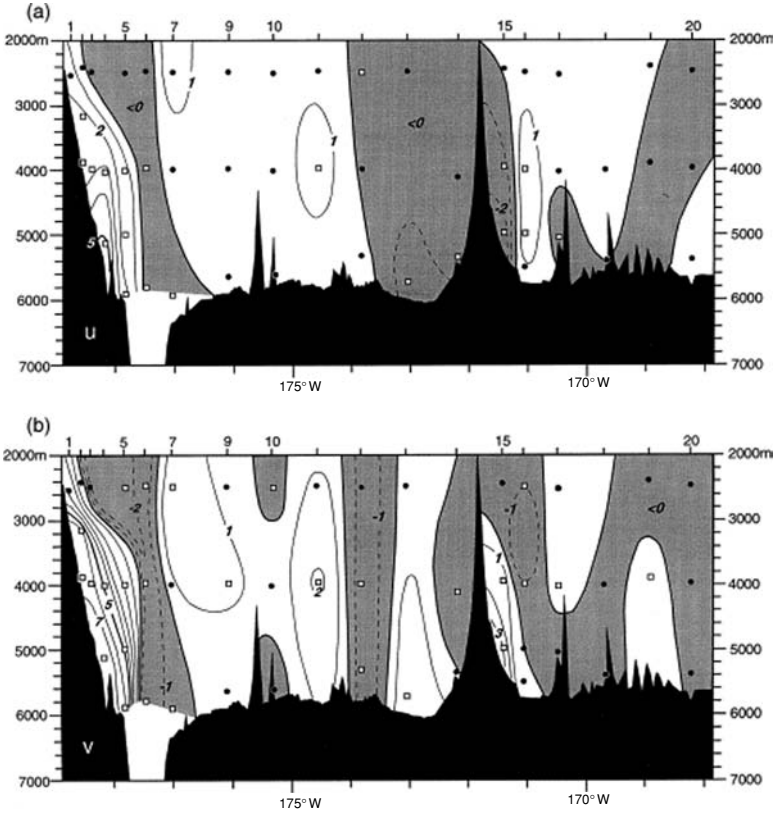

Figure 6.22 (a) The mean zonal velocity from two years of data, and (b) the mean meridional (normal to the section) velocity from two years of direct measurement. Instrument depths are shown as dots. Although there were no measurements above 2000 m, the cellular nature of the mean flow is nonetheless plain. (Source: Whitworth *et al.*, 1999)

for different regions. Ekman fluxes were represented as $\bar{F}_C + \Delta F_C$, where ΔF_C are a new set of unknown adjustments relative to the initial estimates of $\bar{F}_C$. Vertical exchanges were written in the full separated form, Eq. (6.21), but with w^* interpreted as being normal to the isopycnals.

A description of all of the regional constraints is not attempted here because that becomes a discussion of everything that was known, a-priori, about the general circulation, globally. But to give some of the flavor of the procedure, consider only the Pacific Ocean. There, the net northward flux across 17° S and 32° S was constrained to $(7.8 \pm 10) \times 10^9$ kg/s to represent the mass flux previous measurements had suggested were passing into the Bering Sea and into the Indian Ocean north of Australia. At 32° S, current meter measurements were interpreted to demand $(16 \pm 5) \times 10^9$ kg/s moving northward between 179 and 168° W between two of

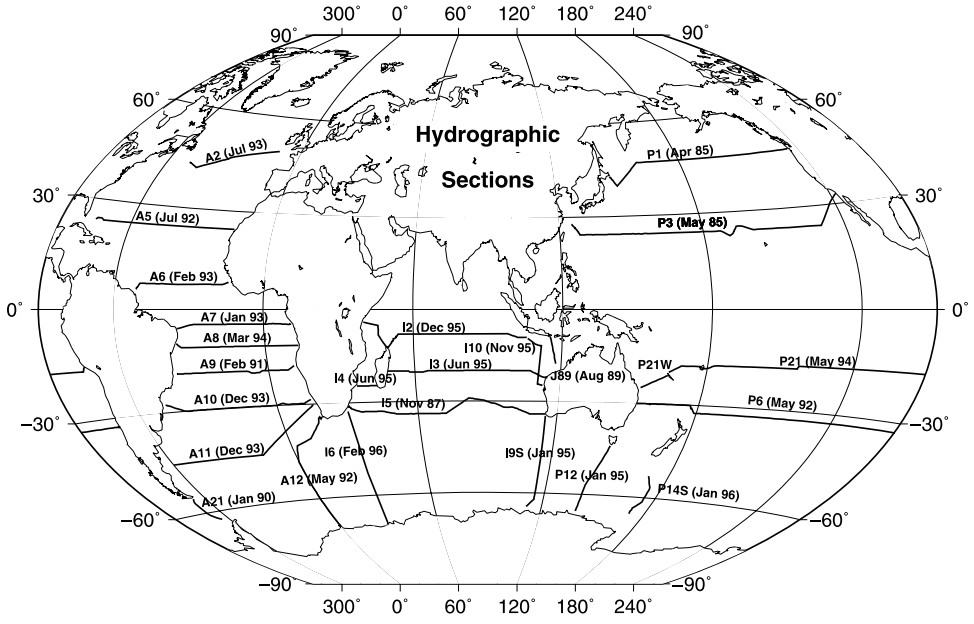

Figure 6.23 Sections defining the volumes of ocean for which property conservation equations were written. (Source: Ganachaud, 2003a)

the isopycnals. Further current meter measurements in the Samoa Passage were used to enforce a mass flux of very cold water to the north of $(12 \pm 4) \times 10^9$ kg/s there. Finally, the reference level, z_0, was chosen to correspond with different isopycnals at different sections, in such a way that a reasonable a-priori estimate of the reference level velocities, b_i, would be zero (see Table 6 of Ganachaud, 2003a).

Similar constraints were written in all ocean basins. As with the regional inversions, one seeks as many constraints, whose accuracy can be quantified, as is possible. The final system was approximately 1200 equations in 3000 unknowns, and solution was by the Gauss–Markov method using the prior error estimates discussed in detail by Ganachaud (2003b). That is, a total of 4200 solution and noise variances were assigned. (An SVD analysis, which is very desirable, involves, e.g., solution resolution matrices, which are 3000×3000 – a size that renders analysis and understanding very difficult.)

A schematic of the final solution is shown in Figs. 6.24 and 6.25. Figure 6.24 displays the total flows (arrows) as integrated across the sections in three layers (sums of the layers used in the inversion) spanning the entire water column. Also shown on the figure are vertical exchanges across the defining interfaces. Figure 6.25 displays the same solution, but showing the horizontal distribution of the flow integrated from west to east (north to south) in the three layers. The interpretation

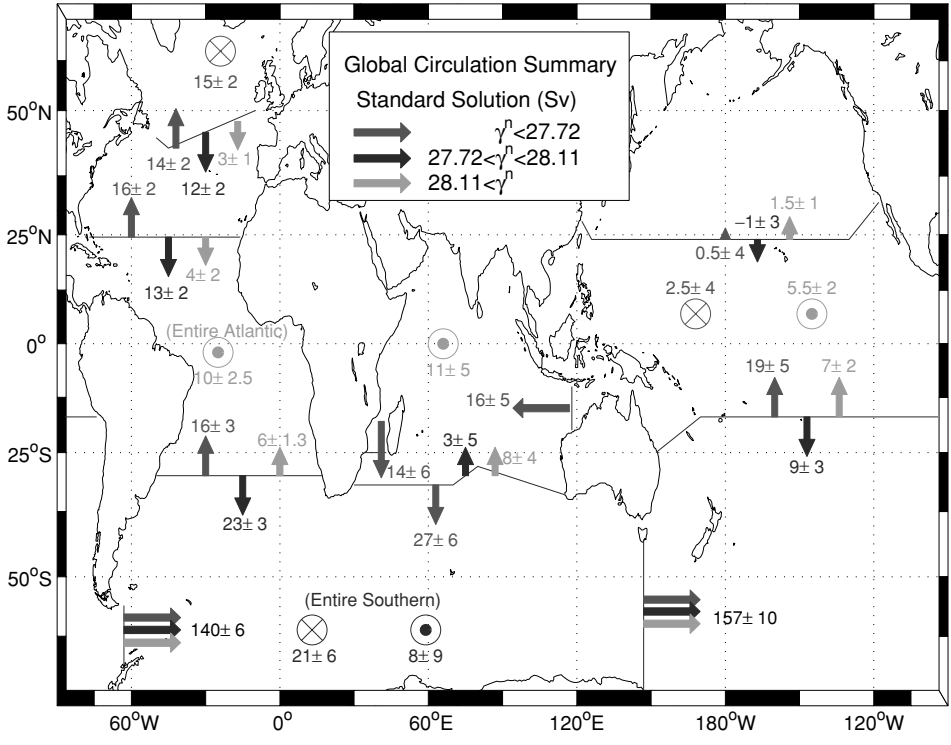

Figure 6.24 Mass flux in the Ganachaud (2003a) solution. Red, blue, and green arrows depict the vertically and horizontally averaged mass flux between the neutral surfaces noted. (See color figs.) (Source: Ganachaud, 2003a)

of these results would take us too deeply into physical oceanography, and the reader is urged to consult the references for further information.

It is worth, however, producing one example of the use of the solution. Figure 6.26 shows the estimated flux of dissolved nitrate in the ocean. Nitrate is a vital biogeochemical field in the ocean, important for both biology and climate. No nitrate constraints were employed in the above solution for the flow and mixing fields and these fluxes were simply computed from the inferred flow field and the observed nitrate distribution. These estimated fluxes (and more important, their divergences) are probably the best available at the present time.

6.4.4 Error estimates

Ganachaud (2003b) revisited the question of specifying the error covariances to be used in large-area box models such as the ones just described. Many sources of error must be accounted for, ranging from internal waves disturbing the density field, to

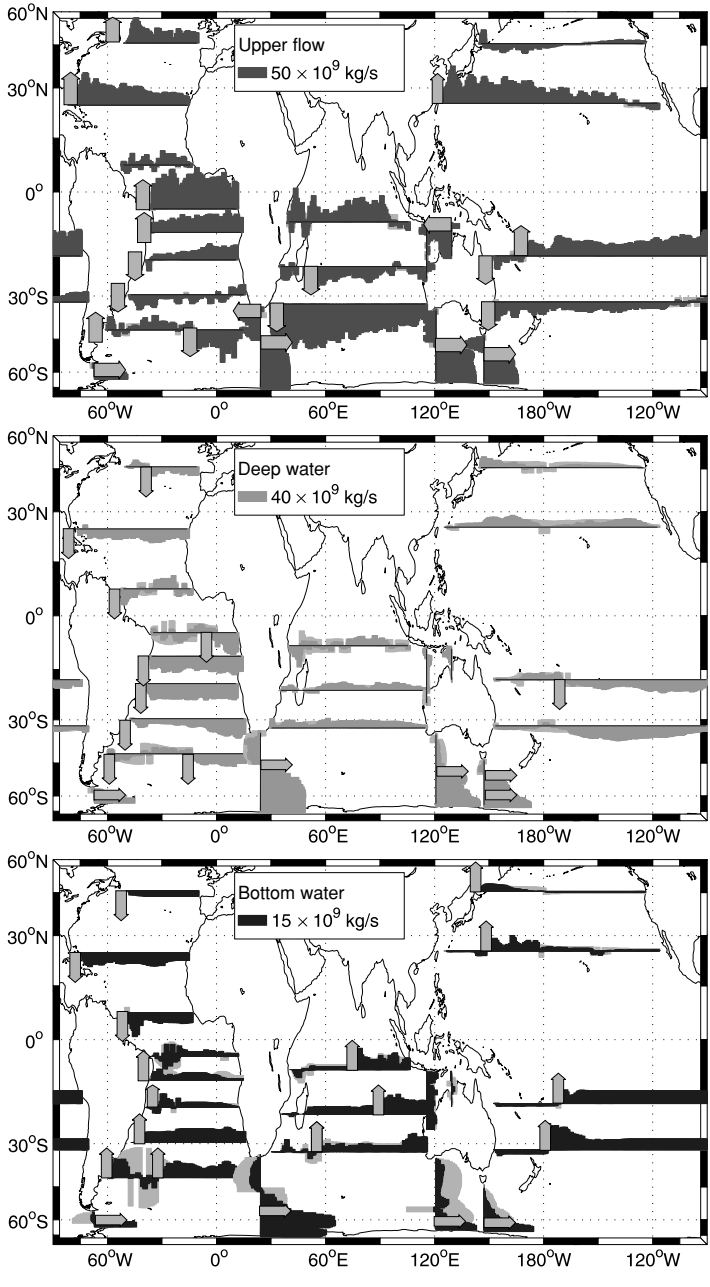

Figure 6.25 Mass transports integrated from west to east and north to south for the solution displayed in Fig. 6.24. Light shading shows the estimated standard errors. Arrows denote the major currents of the system. (See color figs.) (Source: Ganachaud, 2003a)

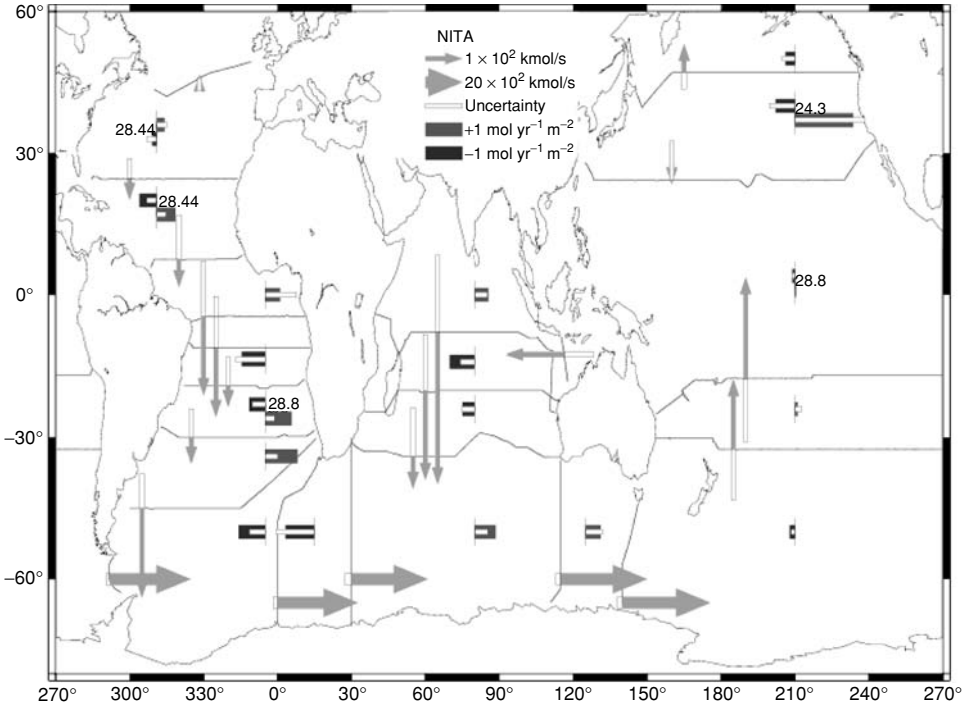

Figure 6.26 Integrated nitrate flux corresponding to the mass flux in Figs. 6.24 and 6.25. Although there is some resemblance to the mass fluxes, significant differences in the net movement of nitrate occur – owing to the spatially varying concentration of nitrate. (See color figs.)

the extrapolation of temperature, salinity, and other properties into regions without data, to instrumental noise, to the finite duration required by a ship to sample the ocean. He relied heavily on the results of a so-called "eddy-permitting" general circulation model, and reference is made to OCIP (Wunsch, 1996) and Ganachaud's paper for further discussion. Perhaps the most significant error, thought to dominate the solutions, is the difference between a flow computed from a quasi-instantaneous ocean sample (a "synoptic" section) and one computed from a hypothetical time average of the flows from sections made over a long period of time. It has been argued (Wunsch, 1978, 1996), that the large-scale spatial integrations of the fluxes involved in the constraint equations might, under an ergodic hypothesis, closely resemble their long-term time average. This hypothesis fails quantitatively, and one cannot, without supplying an error estimate, equate the property fluxes obtained from the box balances to those in a hypothetical time-average ocean. Two separate issues arise: the errors incurred when synoptic sections measured at different times are combined to write regional box balances for any property, and the extent to which the result then can be interpreted as equal to the long-term

average. Both have errors, and they must be carefully evaluated as suggested in the references.

6.4.5 Finite-difference models

Any system that can be put into the standard form $\mathbf{Ex} + \mathbf{n} = \mathbf{y}$ can be solved using the methods of this book. Although the geostrophic box inverse models have usually been written for integrals over large volumes of ocean, the same procedures can be used for the equations in differential form, including, e.g., linear numerical models of the ocean. A simple version was discussed above for generic tracer problems.

As a complement to the above discussion of very large-scale constraints, consider (Martel and Wunsch, 1993b) the use of these methods on a system of equations based upon a discretized generic, steady conservation equation with Laplacian diffusion. That is, consider the partial differential system

$$\mathbf{u} \cdot \boldsymbol{\nabla}(\rho C) - \nabla_{\mathrm{H}}(K_{\mathrm{H}} \nabla(\rho C)) - \frac{\partial}{\partial z}\left(K_{\mathrm{V}} \frac{\partial (\rho C)}{\partial z} \right) = 0, \tag{6.39}$$

subject to boundary conditions (a special case of Eq. (6.1)); K_{H} is the horizontal dimension analogue of K_{V}. To solve such equations in practice, one commonly resorts to numerical methods, discretizing them, e.g., as

$$\begin{aligned}
&\frac{u(i+1,j,k+1/2)\rho C(i+1,j,k+1/2) - u(i,j,k+1/2)\rho C(i,j,k+1/2)}{\Delta x} + \cdots \\
&+ \frac{w(i+1/2,j+1/2,k+1)\rho C(i+1/2,j+1/2,k+1) - w(i+1/2,j+1/2,k)\rho C(i+1/2,j+1/2,k)}{\Delta z} + \cdots \\
&- K_{\mathrm{H}}(i+1,j,k+1/2)\frac{(\rho C(i+1,j,k+1/2) - 2\rho C(i,j,k+1/2) + \rho C(i-1,j,k+1/2))}{(\Delta x)^2} + \cdots \\
&+ n(i,j,k) = 0,
\end{aligned} \tag{6.40}$$

where i, j are horizontal indices, k is a vertical one (x is again here a coordinate, not to be confused with the state vector, $\mathbf{x}$). Compare these to Eqs. (6.4) and (6.5). The $1/2$ index is for a variable evaluated halfway between grid points. ρC_{ijk} is a shorthand for the product of the discretized density and tracer. A discretized form of the mass-conservation equation (6.9) was also written for each unit cell. $n(i, j, k)$ has been introduced to permit the model, Eq. (6.39), to be regarded as imperfect. If $C(i, j, k + 1/2)$ is known at each grid point, the collection of (6.40) plus mass conservation is a set of simultaneous equations for $u(i, j, k + 1/2)$ and K_{xx}, etc. One writes a second finite difference equation corresponding to Eq. (6.9) for mass conservation involving $u(i + 1, j, k + 1/2)$, $v(i, j + 1, k + 1/2)$, $w(i + 1/2, j + 1/2, k + 1), \ldots$.

If the velocity field is calculated using the thermal wind equations on the grid, then at each horizontal grid position, i, j, there is a corresponding pair of unknown reference level velocities $c(i, j)$, $b(i, j)$ as above. This would then be an inverse

problem for a state vector consisting of c, b (and/or K_H, if it is unknown). The equations are in the canonical form, $\mathbf{Ex} + \mathbf{n} = \mathbf{y}$. (In conventional forward modeling, one would specify the u, v, K on the grid and solve the linear equation set (6.40) for $C(i, j, k)$, etc. Here, the problem is inverse because C is known and elements (b, c, K) are the unknowns.) After some rearrangement for numerical convenience, there were about 9000 equations in 29 000 unknowns (the horizontal mixing unknowns were suppressed by giving them zero column weights and are not counted), a system that was solvable by tapered least-squares, taking advantage of the very great sparsity of the equations. The main outcome of this calculation is a demonstration of its feasibility. As the spatial resolution becomes finer, the time-independence assumption fails, and a steady model becomes untenable; that is, it fails on physical grounds. One is driven to employ the models and methods described in Chapter 7.

An interesting study by Tziperman and Hecht (1987) considered a repeated data set that permitted a comparison of solutions from averaged data, as opposed to those from averaging a series of solutions. Unsurprisingly, the results depend upon the order of averaging and calculation, and the differences lead into a discussion of the meaning of the eddy-coefficients, K, not pursued here.

6.5 Linear programming solutions

Linear programming, as outlined in Chapter 3, has been comparatively little used in fluid problems as compared to methods based upon least-squares. The reasons probably lie with its relative unfamiliarity in the physics community and the need to specify rigid upper and lower bounds. The latter appear more demanding than the soft constraints of least-squares, which can be violated. Advantages of linear programming include the very efficient and sophisticated software developed because of widespread economics and management applications; the easy ability to employ semi-qualitative constraints expressing, e.g., the requirement that some field or parameter should be positive or less than some large upper bound; the general insensitivity of 1-norms to data outliers; and the ease of finding absolute upper and lower bounds on interesting properties such as the flux of a scalar across a boundary (Wunsch, 1984). Many software packages automatically produce the dual (or adjoint) solutions, thus providing crucial sensitivity information.

Wunsch (1984) wrote a system of equations like those used in earlier chapters for the geostrophic box inversions but for multiple boxes spanning the North Atlantic. A form suitable for linear programming was used: The soft constraints for mass, salt, etc., conservation were replaced by hard inequalities representing absolute maximum and minimum bounds. Individual bounds were set on the reference-level velocities. The hard bounds did not have any simple statistical

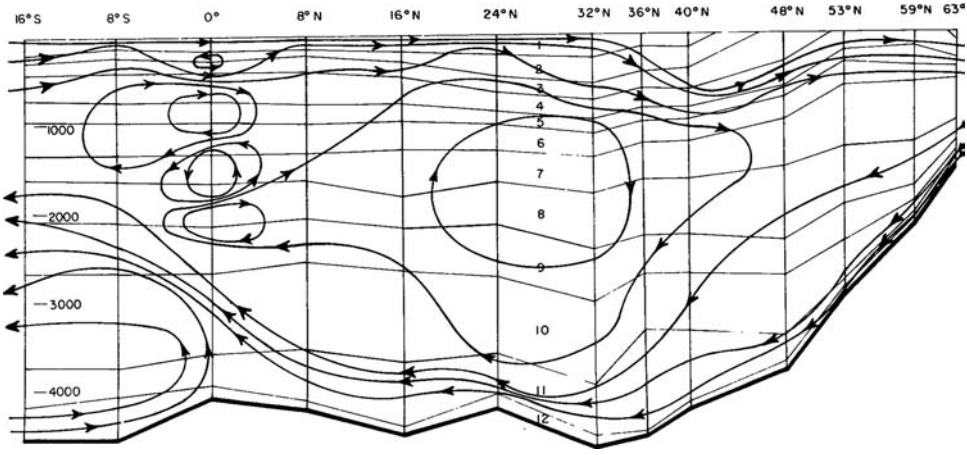

Figure 6.27 Zonal integral of a solution (it is not unique) that maximizes the flux of heat across 24° N in the North Atlantic. The approximate meridional overturning stream function is displayed. (Source: Wunsch, 1984)

interpretation – unlike the soft bounds of Gauss–Markov estimation or least-squares. Rather, they represented partially subjective views, based upon experience, of what would be extreme acceptable values. The objective functions consisted of the heat fluxes across each of the ocean-spanning sections in the form (6.37). As the bounds on x_i are not in linear programming canonical form (they permit both positive and negative values) one introduces new variables, $\mathbf{x}^+$, $\mathbf{x}^-$, which are non-negative, and defines $\mathbf{x} = \mathbf{x}^+ - \mathbf{x}^-$. The result was about 500 constraints in approximately 900 unknown parameters, each with a set of upper and lower bounds (see Eqs. (3.41)–(3.44)).

The problem was solved by a simplex method. The bounding heat fluxes were sought in order to understand their range of uncertainty. One solution that maximizes the net heat flux (including the Ekman component) subject to all of the constraints is depicted in Fig. 6.27.

Such methods, in which bounds are sought, are especially useful in problems that from the point of view of the basic SVD are grossly underdetermined, and for which determining "*the*" value of quantities such as the heat flux is less important than understanding their possible range. If the resulting range is sufficiently small, the remaining uncertainty may be unimportant. For anyone interested in the large-scale properties of the circulation – for example, its chemical and biological flux properties – detailed determination of the flow at any given point may be beyond reach, and not very important, whereas the integrated property extrema may well be well and readily determined. Wunsch (1984) called this approach "eclectic modeling" because inequality constraints are particularly flexible in accounting for the

wide variety and inhomogeneous distribution of most oceanographic observations. These methods (Wunsch and Minster, 1982) are very powerful and, because of the ease with which positivity constraints are imposed, are the natural mathematical tool for handling tracers. Schlitzer (1988, 1989) used linear programming to discuss the carbon budget of the North Atlantic Ocean.

Non-linear extensions of these methods called, generically, "mathematical programming" are also available. One oceanographic example, which involves the adjoint to a general circulation model, is discussed by Schröter and Wunsch (1986), but, thus far, little further use has been made of such techniques.

6.6 The β-spiral and variant methods

6.6.1 The β-spiral

Combinations of kinematic and dynamic equations with observations can be made in many different ways. Take the same governing equations (6.6)–(6.10), but now employ them in a local, differential, mode. The so-called β-spiral method of Stommel and Schott (1977) is a rearrangement of the equations used for the geostrophic box balances, written for a point balance. There are several ways to derive the resulting system.

Ignoring some technical details (chiefly the dependence of density on the pressure), the density equation (6.10) is solved for w, and then differentiated by z,

$$\left(\frac{\partial \rho}{\partial z}\right)^2 \frac{\partial w}{\partial z} = -\left(\frac{\partial \rho}{\partial z}\right)\left(\frac{\partial u}{\partial z}\frac{\partial \rho}{\partial x} + u\frac{\partial^2 \rho}{\partial x \partial z} + \frac{\partial v}{\partial z}\frac{\partial \rho}{\partial y} + v\frac{\partial^2 \rho}{\partial z \partial y}\right) + \left(u\frac{\partial \rho}{\partial x} + v\frac{\partial \rho}{\partial y}\right)\frac{\partial^2 \rho}{\partial z^2}\,. \tag{6.41}$$

Now recognize that the Coriolis parameter f, is a function of latitude. This dependence can be made explicit by writing it in local Cartesian approximation as $f = f_0 + \beta y$, where f_0 and β are constants. Then cross-differentiate the two momentum equations (6.6) and (6.7), which removes the large pressure terms from the system, and, using (6.9),

$$\beta v = f\frac{\partial w}{\partial z}, \tag{6.42}$$

called the "geostrophic vorticity balance." Equation (6.42) permits us to eliminate w from Eq. (6.41). The thermal wind equations (6.17) and (6.18) can be used to write $u(x, y, z) = u_R(x, y, z) + c(x, y)$, $v(x, y, z) = v_R(x, y, z) + b(x, y)$, where u_R, v_R are again assumed known from the density field. Substituting into (6.41)

produces a partial differential equation in ρ involving the integration constants c, b,

$$(u_R + c)\left[\frac{\partial \rho}{\partial x} - \left(\frac{\partial \rho}{\partial z}\right)\frac{\partial^2 \rho}{\partial x \partial z}\right] + (v_R + b)\left[\frac{\partial \rho}{\partial y} - \left(\frac{\partial \rho}{\partial z}\right)\frac{\partial^2 \rho}{\partial z \partial y} - \frac{\beta}{f}\left(\frac{\partial^2 \rho}{\partial z^2}\right)^2\right] = 0\,. \tag{6.43}$$

If b, c were known, Eq. (6.43) would be an equation for the forward problem determining ρ subject to boundary conditions. Instead, one treats ρ as known and attempts to find b, c such that Eq. (6.43) is satisfied at each point x, y, as best possible. If discretized, the result is a set of simultaneous equations for $b(x, y)$, $c(x, y)$ written for different values of z_j, which can be solved by any one of the methods available to us. Suppose that $(x, y) = (x_i, y_i)$ are fixed and that (6.43) is applied at a series of depths $z_i, i = 1, 2, \ldots, M$. There are then M equations in the two unknown $b(x_i, y_i)$, $c(x_i, y_i)$, and a solution and its uncertainty can be found easily. Note again that the coefficient matrix here is constructed from observations, and inevitably contains errors; the full estimation problem would require simultaneously estimating the errors in ρ, and the suppression of that calculation is again a linearization of the full problem implicit in Eq. (6.19).

Figures 6.28–6.30 show the data positions and results of one of the earliest attempts, by Schott and Stommel (1978), to employ the β-spiral ideas in practice. They re-wrote Eq. (6.43) in terms of the isopycnal depth, rather than in terms of the value of the density field at fixed depths, in effect using $z(\rho)$, rather than $\rho(z)$. There are technical reasons for this change having to do with the dependence of ρ on the pressure, but it does not change the character of the equation or of the problem. Note that the greatly underdetermined geostrophic box balance model has been somehow converted into one with apparently arbitrary overdetermination, dependent only upon the number of depths z_i for which one chooses to write Eq. (6.43). How is this possible? By computing the horizontal derivatives in Eq. (6.43) from linear fits over large latitude and longitude ranges of the sections shown in Fig. 6.28, one is, in effect, asserting that b, c are constant over those long distances. An equivalent reduction in the nullspace of the geostrophic box balances could be made either by assigning a very large-scale spatial covariance via $\mathbf{R}_{xx}$ or by adding equations of the form $b_1 = b_2$, $b_2 = b_3$, etc., thus providing equivalent large-scale assumptions (*cf.* Davis, 1978).

When would one use the β-spiral approach as opposed to the large-scale box balances? The answer is chiefly dictated by the available data: the β-spiral requires the ability to determine both the x and y derivatives of the density field, at a central point. The volume integral approach requires derivatives only along sections, as is more commonly available in large-scale ship surveys, but which must define closed

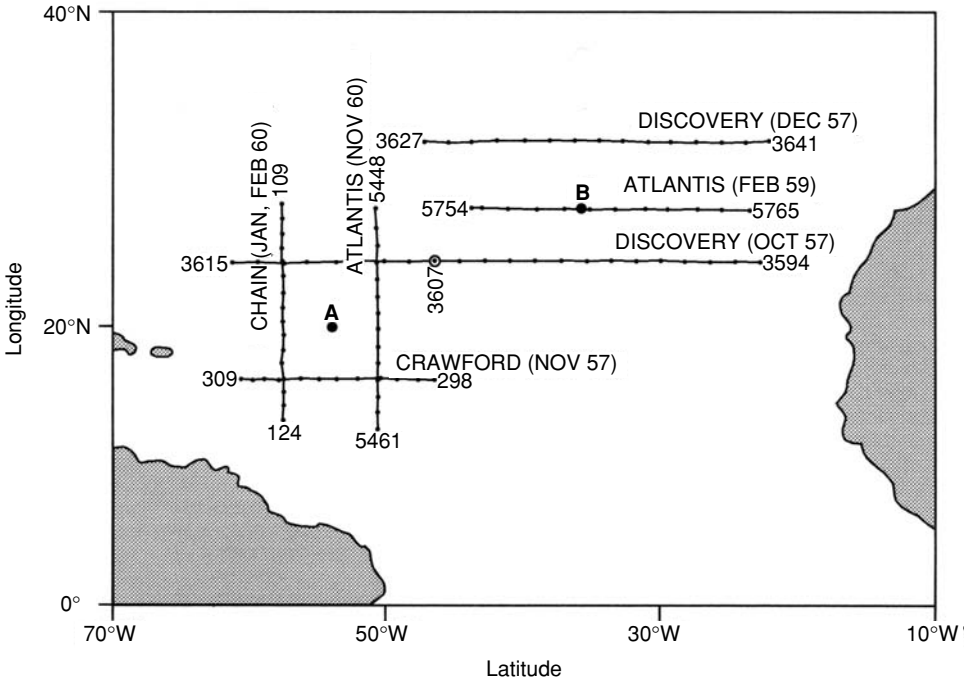

Figure 6.28 Hydrographic sections used by Schott and Stommel (1978) to infer absolute currents at points A,B using the β-spiral constraints. Labels are ship names and dates of measurements; the numbers indicate the ship station number defining the section ends. Isopycnal slopes along the sections are used to estimate the different terms of the β-spiral equations. (Source: after Schott and Stommel, 1978)

volumes. As already noted, one must be very careful about the spatial covariances that may be only implicitly, but nonetheless importantly, present in any attempt to calculate horizontal derivatives. A whole North Atlantic Ocean result for the estimated β-spiral by Olbers *et al.* (1985), based upon a 1° of latitude and longitude climatology, is shown in Fig. 6.31.

In some practical situations, the large-scale box balance constraints have been combined with the point-wise β-spiral balances into one solution (Fukumori, 1991; Ueno and Yasuda, 2003). The non-linear β-spiral problem, accounting for errors, $\Delta\mathbf{E}$, was discussed by Wunsch (1994), and is taken up below.

Many variations on this method are possible. Examples are in Welander (1983), Killworth (1986), Zhang and Hogg (1992), and Chu (1995). These methods might be thought of as hybrids of the straightforward finite difference representations, and the original β-spiral. They have not often been used in practice. Time-dependence in the observed fields remains a major error source, particularly as the regions under study diminish in size.

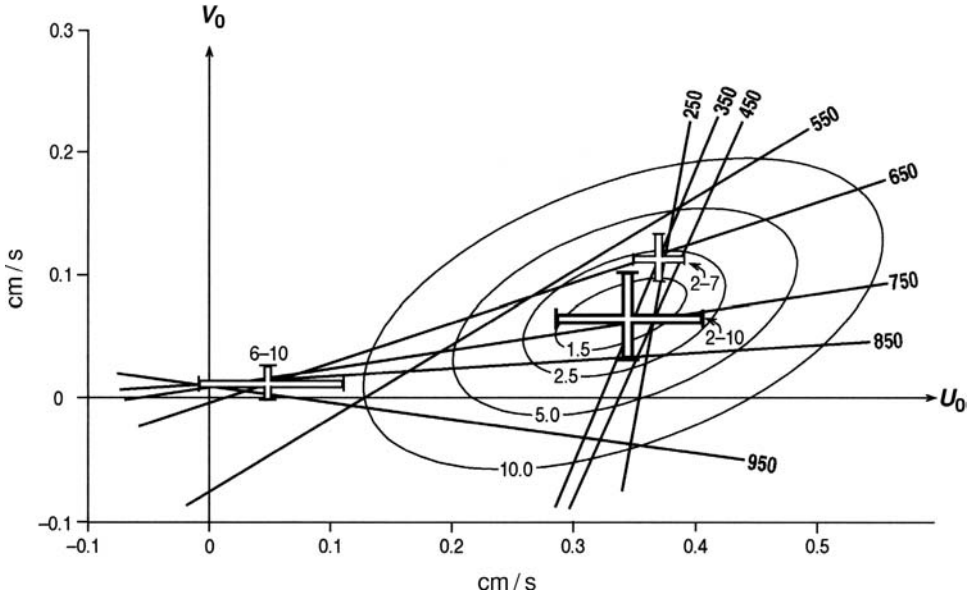

Figure 6.29 β-spiral constraint equations at position B in Fig. 6.28 as a function of depth (numbers on the straight lines). u_0, v_0 correspond to c, b in Eq. (6.43). In the absence of noise, and with a perfect model, the lines should all intersect at a point. Heavy crosses show the best solution over different depth ranges. Error bars are from the equivalent of $\sqrt{\text{diag}\,(\mathbf{P})}$. That the solutions do not agree within error bars suggests that some other physics must also be operative, most probably in the upper ocean depth range.

6.7 Alleged failure of inverse methods

There is a small literature from the early days of the application of inverse methods in physical oceanography, in which various authors claimed to show their failure when applied to the ocean circulation. Unfortunately, the methodologies cannot magically compensate for missing data, or if the model used fails to be consistent with the correct one. The simplest analogy is the one in Chapter 2, attempting to fit a straight line to data actually governed by a higher-order polynomial, or if one grossly misrepresented the noise covariance. The solution is then doomed to be incorrect, not because least-squares or Gauss–Markov methods have failed, but because the problem was incorrectly formulated. Incorrect error covariances can drive a formally correct model away from the correct answer; again one should blame the practitioner, not the tools.

A failure of an inverse method could be claimed if the model relating the observations to the unknowns, $\mathbf{x}$, were fully correct, the prior error covariances were known to be correct, and the estimated solution, $\tilde{\mathbf{x}}$, were then shown to differ from $\mathbf{x}$ beyond the error bars (including the variance of the nullspace, if appropriate).

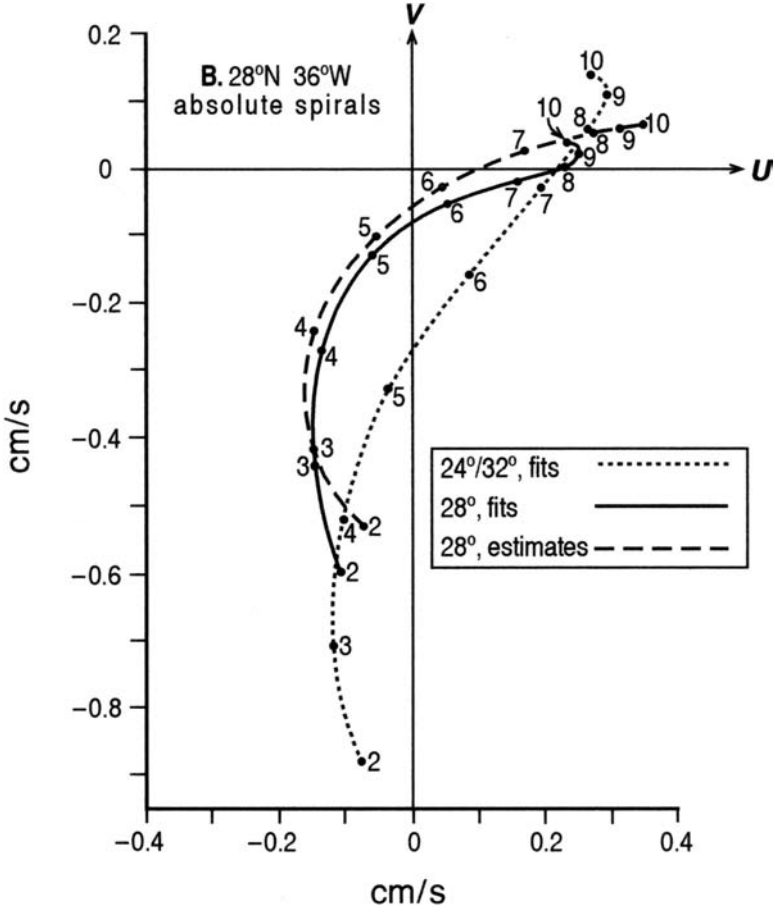

Figure 6.30 Diagram showing the velocity spirals resulting from the solutions to β-spiral equations. Depths are in hundreds of meters. The dashed curve labeled "estimates" is from a visual determination of the isopycnal slopes. The other two curves differ in the central latitude assigned to the Coriolis parameter. (Source: Schott and Stommel, 1978)

Such a failure would be surprising. All of the published claims of failure actually mis-specify a part of the problem in some way, and/or fail to use the uncertainty estimates any inverse method provides.

It sometimes happens that insufficient information is available to resolve some part of the solution of intense interest to a scientist (perhaps he or she seeks the vertical mixing coefficient, K_v); the solution shows it to be poorly resolved (or indistinguishable from zero). Such outcomes have been blamed on the method; but they are the result of *successful* use of the method: one is provided with the specific, and practical information, that more data of certain types would be required to obtain a non-zero estimate.

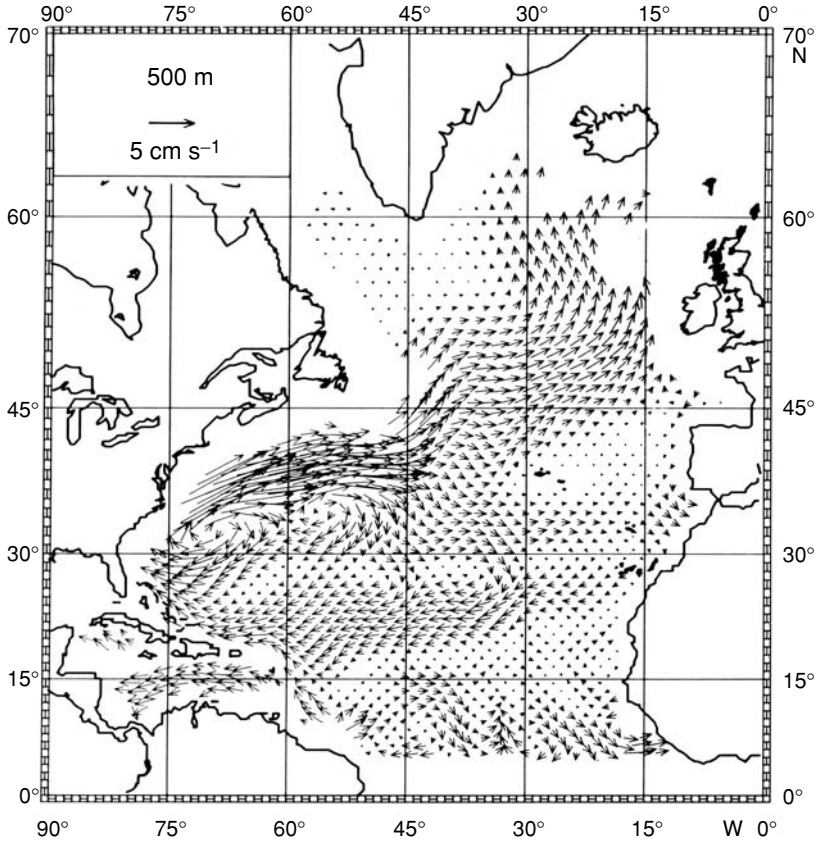

Figure 6.31 Absolute velocity field at 500 m determined from the β-spiral least-squares solution. Straight lines were fit over 1° squares and used a long time-space average to define ρ. (Source: Olbers *et al.*, 1985)

6.8 Applications of empirical orthogonal functions (EOFs) (singular vectors)

Suppose a fluid carries with it a variety of tracer properties. That is, suppose it is tagged by a point in an n-dimensional space of properties, such as temperature, salinity, chlorophyll content, etc. Write the collection of properties at a point as an n-tuple (temperature, depth, horizontal positions (r_x, r_y), salinity, velocity, ...). Oceanographers, with only a two-dimensional display possible on a page, have employed a variety of methods to depict their data. A common one is the section, in which the axes are depth and horizontal distance steamed by a ship, with one property, e.g., temperature, contoured. Another two-dimensional rendering can be obtained by selecting two physical attributes, e.g., temperature and silica concentration, defining those as the graph axes, and plotting each observation on a graph

of temperature versus silica, either as a scatter of points, or sometimes contoured as a histogram. The very large number of possible two-dimensional projections onto planes cutting through the n-space renders it nearly impossible to visualize the properties. There have been a few attempts directed at representations and syntheses more convenient and powerful than property-property diagrams or sections. If one is attempting to understand the degree to which a model is consistent with the real ocean, a measure of distance in one particular two- or three-dimensional subspace of the n-space may give a very distorted picture of the true distance to all of the properties.

Some of the fluid properties that oceanographers measure are nearly redundant, appearing sometimes in geographical space as coincident tongues of, say, salinity and silica, or in property–property space as linear or other simple functional relationships (e.g., the conclusion that salinity is a nearly linear, local, function of temperature). A quantitative description of the relationship becomes useful in several ways: finding an explanation; reducing the dimension of the n-dimensional space; using the relationships to produce estimates of properties of a poorly measured variable from measurements of a better measured one; reducing costs by substituting a cheap-to-measure variable for a functionally connected expensive-to-measure one. Efforts in this direction include those of Mackas *et al.* (1987), Fukumori and Wunsch (1991), Hamann and Swift (1991), Tomczak and Large (1989) and the summary in Bennett (1992). You (2002) describes an application.

Mackas *et al.* (1987), working solely within the physical property space (i.e., the geographical coordinates are ignored), calculated the mixing required to form a particular water type in terms of a number of originating, extreme properties. For example, let the water at some particular place be defined by an n-tuple of properties like temperature, salt, oxygen, etc. $(\theta,\ S,\ O, \ldots)$. It is supposed that this particular set of water properties is formed by mixing a number, N, of parent water masses, for example, "pure" Labrador Sea Water, Red Sea Intermediate Sea Water, etc.,[7] each defined as $[\theta_i,\ S_i,\ O_i, \ldots]$. Mathematically,

$$\begin{aligned}
\theta &= m_1\theta_1 + m_2\theta_2 + \cdots + m_N\theta_N, \\
S &= m_1 S_1 + m_2 S_2 + \cdots + m_N S_N, \\
O &= m_1 O_1 + m_2 O_2 + \cdots + m_N O_N, \\
&\cdots \\
m_1 + m_2 + m_3 + \cdots + m_N &= 1\,,
\end{aligned}$$

and one seeks the fractions, m_i, of each water type making up the local water mass. Because the fractions are necessarily positive, $m_i \geq 0$, the resulting system must be solved either with a linear programming algorithm or one for non-negative least-squares. The equations can as always be rotated, scaled, etc., to reflect prior

statistical hypotheses about noise, solution magnitude, etc. Mackas *et al.* (1987) and Bennett (1992) discuss this problem in detail.

The empirical orthogonal functions as employed by Fukumori and Wunsch (1991) were based directly upon the SVD, using the spatial dimensions. They define a hydrographic station as a column vector of all the properties measured at a station in sequence. That is, let $\boldsymbol{\theta}_i$ be the vector of potential temperatures at station i; let $\mathbf{S}_i$, $\mathbf{N}_i$, etc., be the corresponding $n \times 1$ vector of salinities, nitrate, etc., at that station. Form an extended column vector,

$$\mathbf{s}_i = [[\boldsymbol{\theta}_i]^{\mathrm{T}}, \, [\mathbf{S}_i]^{\mathrm{T}}, \, [\mathbf{N}_i]^{\mathrm{T}}, \ldots]^{\mathrm{T}}$$

(i.e., first n elements are temperatures, second n are salinities, etc.), and make up a matrix of all available hydrographic stations (p of them):

$$\mathbf{M}_2 = \{\mathbf{s}_1, \, \mathbf{s}_2, \ldots, \mathbf{s}_p\}, \tag{6.44}$$

which is a projection of the $N \times n \times p$-dimensional space onto two dimensions. If the SVD is applied to $\mathbf{M}_2$, then, as discussed in Chapter 3, the singular values and $\mathbf{u}_i$, $\mathbf{v}_i$ produce the most efficient possible representation of the matrix. In this context, then either the $\mathbf{u}_i$ or $\mathbf{v}_i$ are empirical orthogonal functions, or principle components. Fukumori and Wunsch (1991) called these the "form-2" modes. If the matrix is ordered instead, as

$$\mathbf{M}_1 = \{\{\boldsymbol{\theta}_i\}, \, \{\mathbf{S}_i\}, \, \{\mathbf{N}_i\} \ldots\}, \tag{6.45}$$

the first n columns of the matrix are the temperatures, the second n are the salinities, etc. These are "form-1" modes. The representation is not unique – it cannot be because a higher-dimensional space is being projected onto a two-dimensional one. More generally, the column and row indices can be time, space, or any ordering or bookkeeping variable. As with the matrices dealt with in earlier chapters, one commonly wishes to introduce various column and row weights before applying the SVD to $\mathbf{M}_1$ or $\mathbf{M}_2$.

6.9 Non-linear problems

The equations of fluid dynamics are non-linear, and sometimes even the most determined linearization cannot adequately represent the physics under consideration. In the geostrophic box models, for example, the coefficient matrix, $\mathbf{E}$, is constructed from observations, and therefore contains a variety of errors, including internal wave noise, ship navigational errors, large-scale time variations, and others. Whether these, and the non-linearities owing to the dynamical simplifications, are truly negligible can only be determined on a case-by-case basis. That the system is non-linear

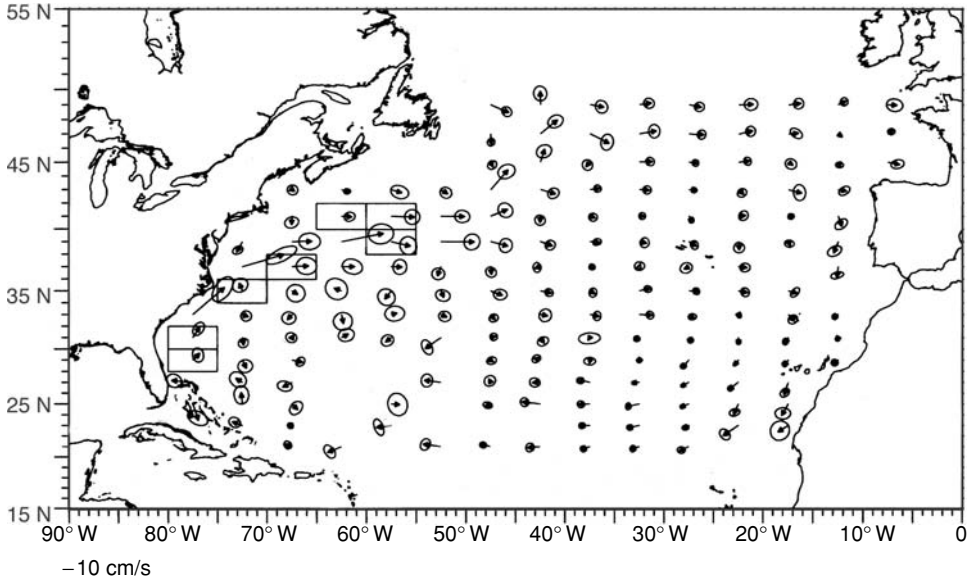

Figure 6.32 Gridded velocity data between about 0 and 100 m depth from neutrally buoyant floats along with an estimated one-standard-deviation error bar, as used in the inverse calculation of Mercier *et al.* (1993). (Adapted from: Mercier *et al.*, 1993)

is implicit in Needler's formula for the absolute velocity. A full representation of the problem of determining the circulation would permit estimation of the density field, simultaneously with the flow and mixing coefficients. This problem has been treated as a non-linear one by Mercier *et al.* (1993) for the North Atlantic time-mean flow.

They first constructed the density field, ρ, as a function of depth and position, and formed the matrix $\mathbf{M} = \{\rho(z, \mathbf{r}_i)\}$, where $\mathbf{r}_i$ is an arbitrary ordering of the station latitudes and longitudes. $\mathbf{M}$ was then approximately represented through Eq. (3.54), the Eckart–Young–Mirsky theorem, in terms of its first ten singular vectors as described in the last section. Each of the EOFs was mapped onto a regular grid using objective mapping and a plausible spatial covariance function. The mapped coefficients of the singular vectors become subject to adjustment. From the mapped density field, one can, using a finite difference scheme, compute the thermal wind (Eqs. (6.15) and (6.16)), and the vertical velocity, w^*, from the thermal wind velocities plus the unknown reference level velocities. In addition to the hydrographic fields, Mercier *et al.* (1993) employed neutrally buoyant float velocities at a variety of levels in the North Atlantic; an example of the gridded values is shown in Fig. 6.32. They wrote an objective function equivalent to

$$J = (\mathbf{d} - \mathbf{d}_0)^{\mathrm{T}} \mathbf{W}_{dd}^{-1} (\mathbf{d} - \mathbf{d}_0) + \mathbf{b}^{\mathrm{T}} \mathbf{W}_{RR}^{-1} \mathbf{b} + (\mathbf{v} - \mathbf{v}_f)^{\mathrm{T}} \mathbf{W}_{ff}^{-1} (\mathbf{v} - \mathbf{v}_f) + \mathbf{m} \mathbf{W}_{mm}^{-1} \mathbf{m}, \tag{6.46}$$

where $\mathbf{d}$ is the vector of coefficients of the hydrographic singular vectors for all vectors at all locations, with initial estimate $\mathbf{d}_0$; $\mathbf{b}$ is the reference level velocity from the thermal wind equations (assumed, initially, as zero); $\mathbf{v}_f$ are the float velocities as gridded; $\mathbf{v}$ is the geostrophic velocity at that depth and location, expressed in terms of the thermal wind, which is a function of $\mathbf{d}$ and the reference level velocity; and $\mathbf{m}$ is the misfit to the dynamical constraint of geostrophic balance and to any other requisite balance (e.g., that surface velocities include an estimated Ekman transport). The $\mathbf{W}_{ii}$ are the usual weight factors, here all diagonal.

The next step is to seek values of $\mathbf{d}$, $\mathbf{v}_R$ that render all terms of J in Eq. (6.46) statistically indistinguishable from 1. $\mathbf{d}$ occurs, implicitly, in $\mathbf{m}$. Because the density is being modified, the problem is fully non-linear. To proceed, Mercier *et al.* (1993) used a quasi-Newton descent method suggested by Tarantola and Valette (1982), but any good minimization algorithm would do (see, e.g., Press *et al.*, 1996). They succeeded in finding a generally acceptable solution (there are inevitable discrepancies). The resulting flow, away from the Ekman layer, is consistent with all the data used and with geostrophic hydrostatic balance.

A somewhat different non-linear hydrographic inversion was described by Wunsch (1994) for a generalization of the β-spiral problem discussed above. In the β-spiral, Eq. (6.43) was solved in a simple overdetermined, least-squares form, leaving residuals in each layer of the water column. Suppose, however, that small adjustments to the observed density field could be found such that the residuals were reduced to zero at all depths. The result would then be an estimate not only of the velocity field but of a density field that was completely consistent with it, in the sense that Eq. (6.6)–(6.10) would be exactly satisfied.

To proceed, Wunsch (1994) wrote the β-spiral equation using the pressure field rather than isopycnal layer depths, and in spherical coordinates. Put

$$P \equiv \frac{p}{\rho_0} = -g \int_{z_0}^{z} \frac{\rho}{\rho_0} \mathrm{d}z + P_0(\phi, \lambda), \tag{6.47}$$

where P_0 is an (unknown) reference pressure, and then Eqs. (6.6)–(6.10) can be written as

$$\begin{aligned} &\frac{\partial P}{\partial \phi}\left(\frac{\partial^3 P}{\partial z^3}\frac{\partial^2 P}{\partial \lambda \partial z} - \frac{\partial^2 P}{\partial z^2}\frac{\partial^3 P}{\partial \lambda \partial z^2}\right) \\ &\quad + \frac{\partial P}{\partial \lambda}\left(\frac{\partial^2 P}{\partial z^2}\frac{\partial^3 P}{\partial \phi \partial z^2} - \frac{\partial^3 P}{\partial z^3}\frac{\partial^2 P}{\partial \phi \partial z} + \cot\phi\left(\frac{\partial^2 P}{\partial z^2}\right)^2\right) \\ &\quad = K 2\Omega a^2 \sin\phi \cos\phi \left(\frac{\partial^2 P}{\partial z^2}\frac{\partial^4 P}{\partial z^4} - \left(\frac{\partial^3 P}{\partial z^3}\right)^2\right), \end{aligned} \tag{6.48}$$

where ϕ is latitude, λ is longitude, and K is a vertical-eddy coefficient, assumed to be constant in the vertical in deriving (6.48). Equation (6.48) was derived by Needler (1967) and is sometimes known, along with $K = 0$, as the "P-equation." Its correspondence with the β-spiral equation was not noticed for a long time.

Substitution of an observed density field and a plausible initial reference pressure, $\tilde{P}_0(0, \phi, \lambda)$, into (6.48) results in large values for K, which is here regarded as a model/data residual rather than as a manifestation of real mixing. Choosing P_0 is the same as having to choose an initial reference level in conventional dynamic computations. The problem was converted to an optimization one by asserting that K appears finite only because the initial reference-level velocity of zero is not correct and because there are also errors in the observed density field, called $\tilde{\rho}(0, \phi, \lambda)$.

Both $\tilde{P}_0$ and $\tilde{\rho}$ were expanded in a three-dimensional set of Chebyschev polynomials, whose coefficients a_{nm}, α_{nml} respectively, become the parameters $\mathbf{x}$. The objective function, J, was formed by computing the sum of squares of K calculated on a three-dimensional grid:

$$J = \sum_{ijk} (\tilde{K}_{ijk} \sin \phi_{ij} \cos \phi_{ij})^2 + R_r^{-2} \sum_{ijk} (\tilde{\rho}_{ijk}(1) - \tilde{\rho}_{ijk}(0))^2 . \tag{6.49}$$

The indices, ijk, refer to the horizontal and vertical grid positions where the expression (6.49) is evaluated after substitution of the Chebyschev expansion. The terms in $\tilde{\rho}$ penalize deviations from the initial estimates with a weight given by R_r. The index, 1, in the argument denotes the modified estimate.

If the coefficients of $\tilde{\rho}$ are held fixed at their initial values as determined from the observations, then only the reference pressure is being optimized. The normal equations in that case are linear, and one is simply solving the ordinary β-spiral problem. The search for an improved density/pressure estimate was carried out using a so-called Levenburg–Marquardt method (e.g., Gill *et al.*, 1986), and a minimum was found. The uncertainty of the final solution was then estimated using the Hessian evaluated in its vicinity. The final residuals are not zero, but are sufficiently small that the solution was deemed acceptable. Because slight changes in the prior density field are capable of producing a solution that implies conservation of potential vorticity, density, etc., within uncertainty limits, the result suggests that estimates of vertical mixing coefficients in the ocean differing from zero may well be nothing but artifacts of sampling errors. Davis (1994) draws a similar conclusion from entirely different reasoning.

Notes

1 *The Ocean Circulation Inverse Problem* (Wunsch, 1996).
2 Brief histories of the use of inverse methods for determing the oceanic general circulation can be found in OCIP (Wunsch, 1996), and in Wunsch (1989).

3 See for example, Pedlosky (1987).
4 The geostrophic flow is also largely due to the wind driving, but much more indirectly than is the Ekman component.
5 We will also ignore, for simplicity, the estimated 0.8×10^9 kg/s flowing southward across all sections and representing the inflow from the Arctic (and ultimately from the North Pacific). Including it raises no new issues.
6 In a more exact configuration, one would use so-called neutral surfaces (Jackett and McDougall, 1997), but the practical difference in a region such as this is slight.
7 Attaching pet names to water types is not necessary, but it is a tradition and gives many oceanographers a sense of intimacy with their subject, similar to the way physicists define quarks as having charm, and it does provide some geographic context.